TITLE:

Chemical bonding and nonadiabatic electron wavepacket dynamics in densely quasi-degenerate excited electronic state manifold of boron clusters

AUTHOR(S):

Arasaki, Yasuki; Takatsuka, Kazuo

CITATION:

Arasaki, Yasuki ...[et al]. Chemical bonding and nonadiabatic electron wavepacket dynamics in densely quasi-degenerate excited electronic state manifold of boron clusters. The Journal of Chemical Physics 2019, 150(11): 114101.

ISSUE DATE:

2019-03-21

URL:

http://hdl.handle.net/2433/237498

RIGHT:

© 2019 Author(s). All article content, except where otherwise noted, is licensed under a Creative Commons Attribution (CC BY) license (http://creativecommons.org/licenses/by/4.0/).

京都大学学術情報リポジトリ
KURENAI 紅
Kyoto University Research Information Repository

京都大学 KYOTO UNIVERSITY

A Self-archived copy in
Kyoto University Research Information Repository
https://repository.kulib.kyoto-u.ac.jp

京都大学学術情報リポジトリ KURENAI 紅
Kyoto University Research Information Repository

The Journal of Chemical Physics

Chemical bonding and nonadiabatic electron wavepacket dynamics in densely quasi-degenerate excited electronic state manifold of boron clusters

Cite as: J. Chem. Phys. **150**, 114101 (2019); https://doi.org/10.1063/1.5094149
Submitted: 28 December 2018 . Accepted: 26 February 2019 . Published Online: 15 March 2019

Yasuki Arasaki, and Kazuo Takatsuka

openaccess

View Online Export Citation CrossMark

ARTICLES YOU MAY BE INTERESTED IN

Accurate excited-state energetics by a combination of Monte Carlo sampling and equation-of-motion coupled-cluster computations
The Journal of Chemical Physics **150**, 111101 (2019); https://doi.org/10.1063/1.5090346

Ultrafast photodissociation dynamics and nonadiabatic coupling between excited electronic states of methanol probed by time-resolved photoelectron spectroscopy
The Journal of Chemical Physics **150**, 114301 (2019); https://doi.org/10.1063/1.5079549

Linear scaling algorithm for tight-binding molecular dynamics simulations
The Journal of Chemical Physics **150**, 114107 (2019); https://doi.org/10.1063/1.5088918

AIP Publishing

© 2019 Author(s).

京都大学 KYOTO UNIVERSITY
A Self-archived copy in
Kyoto University Research Information Repository
https://repository.kulib.kyoto-u.ac.jp
京都大学学術情報リポジトリ KURENAI 紅 Kyoto University Research Information Repository

The Journal of Chemical Physics ARTICLE scitation.org/journal/jcp

Chemical bonding and nonadiabatic electron wavepacket dynamics in densely quasi-degenerate excited electronic state manifold of boron clusters

Cite as: J. Chem. Phys. 150, 114101 (2019); doi: 10.1063/1.5094149
Submitted: 28 December 2018 • Accepted: 26 February 2019 •
Published Online: 15 March 2019

View Online Export Citation CrossMark

Yasuki Arasaki and Kazuo Takatsuka[a)]

AFFILIATIONS

Institute for Fundamental Chemistry, Kyoto University, 606-8103 Kyoto, Japan

[a)]Electronic mail: kaztak@fukui.kyoto-u.ac.jp

ABSTRACT

Formation of chemical bonds is theoretically discerned by the presence of static nuclear configuration on a potential energy surface given within the Born–Oppenheimer framework. We here study dynamical chemical bonding for molecules residing in the electronic excited states that are in a densely quasi-degenerate electronic state manifold and thereby keep undergoing extremely frequent nonadiabatic transitions. For this type of the states, the notion of global potential energy surfaces based on the adiabatic representation loses the usual sense. Nonetheless, chemical bonding exists and associated chemical reactions certainly proceed, for which we call chemistry without potential surfaces. As such, we investigate the highly excited states of boron clusters, which have extraordinarily long lifetimes with neither ionization nor dissociation. The dynamical chemical bonds keep rearranging themselves without converging to a static structure, the vivid electron dynamics of which is tracked by means of the nonadiabatic electron wavepacket dynamics theory. To characterize the dynamical bonding theoretically, we propose the notion of hyper-resonance.

© 2019 Author(s). All article content, except where otherwise noted, is licensed under a Creative Commons Attribution (CC BY) license (http://creativecommons.org/licenses/by/4.0/). https://doi.org/10.1063/1.5094149

I. INTRODUCTION

Rigorous definition of chemical bond, irrespective of the kind such as covalent, ionic, and so on, is usually given such that nuclei in an atomic aggregate can all sit at a minimum (local or global) on the quantum chemical potential energy surface, and thereby the classical forces working on the nuclei are everywhere zero. Besides, the quantum vibrational states can/should be formed around the bottom of the relevant potential basin. This definition is very general and can be rigorously verified as far as the ground state molecules are concerned. Note that this quantum chemical definition totally rests on the Born–Oppenheimer view of molecules.[1,2] In this paper, we discuss a characteristic chemical bonding to be identified only in the molecular realm beyond the Born–Oppenheimer paradigm.[3–7]

In contrast to the above quantum chemical definition, far more flexible and less rigorous definition of chemical bonding was proposed by Pauling in his *The Nature of the Chemical Bond*,[8] from which it is quoted "We shall say that there is a chemical bond between two atoms or groups of atoms in case that the forces acting between them are such as to lead to the formation of an aggregate with sufficient stability to make it convenient for the chemist to consider it as an independent molecular species." This proposal made in the very early stage of theoretical chemistry turns out to get wider popularity in the present age of excited state chemistry and ultrafast chemical dynamics, the progress of which is greatly assisted by laser technology.[9,10] For instance, it has been theoretically found that alkali halides such as LiF placed in an appropriate continuous wave (CW) laser field can have a very long lifetime (far longer than 1 ps) in the Franck–Condon region with energy higher than the dissociation limit.[11] One picosecond lifetime, at the shortest, is long enough for scientists in dynamics to consider it sufficiently stable and convenient to regard it as an independent

© Author(s) 2019

京都大学 KYOTO UNIVERSITY
A Self-archived copy in
Kyoto University Research Information Repository
https://repository.kulib.kyoto-u.ac.jp
京都大学学術情報リポジトリ KURENAI 紅 Kyoto University Research Information Repository

molecular species.[9,10] The basic mechanism of this "molecular formation" can be simply summarized as follows. The CW laser field makes many copies of the so-called dressed-states from the original (undressed) one, concomitantly generating the corresponding potential curves of the ionic character, say, (Li^+–F^-, $n\hbar\nu$), each of which can have an avoided crossing with that of the covalent nature (Li–F). Those dressed potential curves of the ionic nature can have high dissociation energy since they are lifted high above the original curve. The nuclear wavepackets running toward the dissociation channel on the covalent curve encounter thus created dressed ionic curves many times and they bifurcate into them at each encounter. The bifurcated waves are brought back to the Franck–Condon region after hitting the turning points on the individual dressed curves. This dynamical state confined in the Franck–Condon region can have a very long lifetime under an appropriate condition, which may be therefore termed laser-assisted nonadiabatic chemical bonding.

The laser assisted confined state will be immediately eliminated by switching off the laser. Besides, one has to align the molecules' orientation with respect to the laser polarization vectors. However, one may anticipate that molecules having densely quasi-degenerate electronic states and thereby undergoing very frequent and continual nonadiabatic transitions can have an extremely long lifetime even with no assistance of laser fields. An illuminating example is the electronically excited states of boron clusters. In these molecules, the dissociation channels are closed efficiently not by the dressed states but by frequent nonadiabatic transitions in other vibrational modes that are transversal to the dissociation coordinates. We may call these states dynamical chemical bonding and/or hyper-resonance states. By definition which will be given later, these states can appear only in the molecular regime beyond the Born–Oppenheimer framework. The present paper is devoted to the precise presentation of the characteristics of the dynamical bonding and the theoretical analysis of the hyper-resonance.

Boron containing molecules are well-known to have very characteristic chemical bonding even in the ground electronic state, which is referred to as electron-deficient or hypervalent bond. There have been many studies on the chemical bonding, molecular structure, and chemical reactivity of molecules containing boron atoms in them. Among others, Lipscomb and his co-workers are the pioneers for the systematic and extensive studies on the molecular geometry of boron compounds such as diborane.[12–17] Highly active chemical reactions in hydroboration has been studied by Brown and his colleagues,[18,19] and the use of boron in chemical synthesis is still an ongoing area of research.[20,21] There are many other important studies on boron chemistry in the literature, the science of boron nitride polymer[22] being a well-known example. Boron has numerous uses in various fields of science: as clusters,[23] as radicals,[24] as metal-free catalysts,[25] in superconductivity,[26,27] hydrogen storage,[28] luminescent materials,[29] dendrimers,[30] batteries,[31] and in biological probing and medicine[32,33] to name but a few recent examples. The uniqueness of boron stems one way or another from its electron-deficient nature, whose basic characteristics may be studied in the structure of small boron clusters.[34–41] Electron dynamics in boron has been much less studied.[42,43] Yonehara and Takatsuka are among the first who have investigated the electron dynamics of highly excited states of boron clusters as a primary target of a nonadiabatic electron wavepacket study.[44] These authors described the very basic properties of the clusters such as the diffusion-like behavior of the electronic states in the state space. Various quantities were computed in an attempt to survey and characterize the molecular properties which had not been previously observed. The present paper follows this paper, placing a particular emphasis on the chemical bonding assisted by the frequent nonadiabatic dynamics, which is far from the concept of chemical bond in the Born–Oppenheimer paradigm.

The present work is concerned about chemical and physical consequences of molecular nonadiabatic interactions.[3–7] However, unlike the canonical studies on nonadiabatic transitions, our target is not to estimate the nonadiabatic transition probabilities. In the very frequent nonadiabatic dynamics among so many electronic states in the densely quasi-degenerate manifold, counting the transition probabilities by means of the one-dimensional nonadiabatic theories like the Landau–Zener theory is neither interesting nor relevant. The most important scientific aspect here is to continuously track electron dynamics driven by the nonadiabatic interactions in order to extract the essential natures of chemical dynamics and bonding in such extremely quasi-degenerate electronic manifolds. The theory of nonadiabatic electron wavepacket dynamics provides a practical method to enable the deepening of chemical insights.[6,7]

This paper is structured as follows. Section II first presents the practical methods we apply in this work. Some basic quantities are shown such as the local properties of the potential energy surfaces of the excited states of boron clusters in Sec. III. Section IV demonstrates the very characteristics of what we call the dynamical chemical bonding of the excited states. Summarizing the numerical studies, we propose in Sec. V a notion of hyper-resonance or dynamical bonding to characterize thus revealed chemical bonding. The paper concludes in Sec. VI.

II. THEORETICAL METHODS

This section introduces an outline of the theory with which we numerically study the nonadiabatic electron wavepacket dynamics.

A. Nonadiabatic electron dynamics

We aim to follow the excited state dynamics of the B_{12} cluster, where adiabatic electronic states are quasi-degenerate and highly mixed and thereby nonadiabatic transitions take place extremely frequently, practically, in the order of once in every femtosecond.[42,44] To track nonadiabatic electron dynamics, we have developed a theory of path-branching representation. The basis of the theory is described in Refs. 45–47 and in review articles.[6,7,48] The theory has been extended for laser chemistry,[49–51] for electron dynamics in condensed phases,[52] and photoionization dynamics.[53–55] A very characteristic symmetry property of nonadiabatic dynamics is discussed in Ref. 56. The aspect of quantization of the associated nuclear paths is also studied in Refs. 57 and 58.

We start with the outline of the path-branching representation. The standard nonrelativistic full dimensional electronic and nuclear Hamiltonian is usually written as

$$\hat{H}(\boldsymbol{r},\boldsymbol{R}) = \frac{1}{2}\sum_k \hat{P}_k^2 + \hat{H}^{(\mathrm{el})}(\boldsymbol{r};\boldsymbol{R}), \tag{1}$$

© Author(s) 2019

京都大学 KYOTO UNIVERSITY
A Self-archived copy in
Kyoto University Research Information Repository
https://repository.kulib.kyoto-u.ac.jp
京都大学学術情報リポジトリ KURENAI 紅 Kyoto University Research Information Repository

where $H^{(el)}(\boldsymbol{r};\boldsymbol{R})$ is the electronic Hamiltonian for the electronic $\boldsymbol{r}$ and nuclear $\boldsymbol{R}$ coordinates with $\hat{P}_k$ being the quantum mechanical momentum operator associated with R_k, the kth component of $\boldsymbol{R}$. This electronic and nuclear Hamiltonian is equivalently rewritten as

$$\hat{H} = \frac{1}{2}\sum_k \left\{ \hat{P}_k - i\hbar \sum_{IJ} |\Phi_I(\boldsymbol{R})\rangle X^k_{IJ}(\boldsymbol{R}) \langle \Phi_J(\boldsymbol{R})| \right\}^2 + \sum_{I,J} \left|\Phi_I(\boldsymbol{R})\right\rangle H^{(el)}_{IJ}(\boldsymbol{R}) \left\langle \Phi_J(\boldsymbol{R})\right|, \tag{2}$$

where $H^{(el)}_{IJ}(\boldsymbol{R})$ is the matrix representation of the electronic Hamiltonian $\hat{H}^{(el)}(\boldsymbol{r};\boldsymbol{R})$ in the chosen basis set and the first order kinematic interaction between the basis functions in the direction of the kth degree of freedom $X^k_{IJ}(\boldsymbol{R})$ is defined as

$$X^k_{IJ}(\boldsymbol{R}) = \langle \Phi_I(\boldsymbol{R}) | \frac{\partial}{\partial R_k} | \Phi_J(\boldsymbol{R}) \rangle_{\boldsymbol{r}}. \tag{3}$$

The total electronic wavefunction $\Psi_{elec}(\boldsymbol{r}, t, \boldsymbol{R}(t))$ is to be propagated in time along nuclear paths $\boldsymbol{R}(t)$, which is simultaneously determined according to the matrix force described below. $\Psi_{elec}(\boldsymbol{r}, t, \boldsymbol{R}(t))$ is expanded in real basis functions $\{\Phi_I(\boldsymbol{r};\boldsymbol{R})\}$ at each nuclear configuration $\boldsymbol{R}(t)$ in such a way that

$$\Psi_{elec}(\boldsymbol{r}, t, \boldsymbol{R}(t)) = \sum_I C_I(t)\, \Phi_I(\boldsymbol{r};\boldsymbol{R})|_{\boldsymbol{R}=\boldsymbol{R}(t)}, \tag{4}$$

where $\{C_I(t)\}$ are complex-valued expansion coefficients. The electronic basis functions are defined on a set of time evolving nuclear paths $\boldsymbol{R}(t)$. We time evolve the expansion coefficients taking the nonadiabatic interactions between the basis functions into account such that

$$i\hbar \frac{\partial}{\partial t} C_I(t) = \sum_J \left[H^{(el)}_{IJ}(\boldsymbol{R}(t)) - i\hbar \sum_{k=1}^{3N} \left(\dot{R}_k(t) X^k_{IJ} - \frac{\hbar^2}{4}\left(Y^k_{IJ} + Y^{k*}_{JI} \right) \right) \right] C_J(t), \tag{5}$$

where N is the number of nuclei and the second order nuclear derivative coupling terms Y^k_{IJ} defined as

$$Y^k_{IJ}(\boldsymbol{R}(t)) = \langle \Phi_I(\boldsymbol{r};\boldsymbol{R}(t)) | \frac{\partial}{\partial R_k^2} | \Phi_J(\boldsymbol{r};\boldsymbol{R}(t)) \rangle_{\boldsymbol{r}} \tag{6}$$

are nontrivial corrections[45] to the electron dynamics and the standard semiclassical Ehrenfest theory (SET) (see below). As is often the case, however, we neglect the second order couplings $Y^k_{IJ}(\boldsymbol{R}(t))$ as they enter only through a factor of $\hbar^2$ [cf. Eq. (4) of previous work[44]].

The nuclear motion is to be driven by the force matrix (an extension of the Newtonian force)[45]

$$\begin{aligned} F^k_{IJ}(\boldsymbol{R}(t)) &= \langle \Phi_I(\boldsymbol{r};\boldsymbol{R}(t)) | \frac{\partial \hat{H}^{(el)}(\boldsymbol{r},\boldsymbol{R})}{\partial R_k} | \Phi_J(\boldsymbol{r};\boldsymbol{R}(t)) \rangle_{\boldsymbol{r}} \\ &= \sum_K \left[X^k_{IK}(\boldsymbol{R}(t)) H^{(el)}_{KJ}(\boldsymbol{R}(t)) - H^{(el)}_{IK}(\boldsymbol{R}(t)) X^k_{KJ}(\boldsymbol{R}(t)) \right] \\ &\quad + \frac{\partial H^{(el)}_{IJ}(\boldsymbol{R}(t))}{\partial R_k}, \end{aligned} \tag{7}$$

which is derived in the mixed quantum and classical representation of the Hamiltonian of Eq. (2). The expansion in the second line of Eq. (7) is appropriate even in the case of an incomplete basis set.[45] The force matrix $F^k_{IJ}(\boldsymbol{R}(t))$ can be generally applied to the nonadiabatic branching of a nuclear path $\boldsymbol{R}(t)$ into many pieces,[6,7,48] which mimics the full quantum mechanical wavepacket bifurcation taking place across nonadiabatic regions. (See Ref. 59 for a direct observation of wavepacket bifurcation in terms of the time-resolved photoelectron spectroscopy.)

However, many excited states of boron clusters to be studied in this paper are densely packed (quasi-degenerate) in a narrow energy range, thereby bearing statistical nature in the electronic state manifold (or in the Hilbert space). In such cases, discussions based on the notion of isolated adiabatic (diabatic as well) states lose the sense. It is therefore not only intractable but also not very meaningful to faithfully track the very many (theoretically infinite) cascade-like branching paths. Besides, the dynamics of electronic-configuration mixing is much faster than the nuclear motion, and furthermore, our studied B_{12} clusters remain bounded for very long time. In order to track electronic state mixing in such an extreme situation, the semiclassical Ehrenfest theory (SET) based method should be a good starting point for short time (up to hundreds of fs) dynamics. Hence, our strategy here is to run plural averaged paths (SET paths) to track the electronic states in detail. A little more sophisticated approximation is to take account of branching of those SET paths at every given running-time, say, 10 fs. This aspect will be discussed in our future reports.

In the SET, the set of nuclear coordinates $\boldsymbol{R}(t)$ and momenta $\boldsymbol{P}(t)$, identified with the time derivative of the coordinates in Eq. (5),

$$P_k(t) = m_k \dot{R}_k(t) \tag{8}$$

are to be time evolved through wavepacket averaged force,

$$m_k \ddot{R}_k(t) = -\sum_I \sum_J C^*_I(t) F^k_{IJ}(\boldsymbol{R}(t)) C_J(t). \tag{9}$$

SET and their extensions with an accurate estimate of the multidimensional nonadiabatic coupling elements $X^k_{IJ}(\boldsymbol{R}(t))$ have been extensively used in the investigation of low-lying excited-state dynamics.[60–64]

We numerically integrate Eqs. (5) and (9) simultaneously: Eq. (9) by the velocity Verlet method[65] and at each time step diagonalizing the bracketed expression in Eq. (5). Since the adiabatic electronic states lose significance in the highly mixed region we consider, we take the configuration state functions (CSFs) as the basis functions $\{\Phi_I(\boldsymbol{r};\boldsymbol{R})\}$. The CSFs are generated at each time step from molecular orbitals obtained at the set of nuclear coordinates $\boldsymbol{R}(t)$ with the restricted Hartree–Fock method. A very careful treatment should be performed to correctly connect the electronic configurations $\Phi_I(\boldsymbol{r};\boldsymbol{R}(t))$ and its counterpart after a short time interval Δt, that is, $\Phi_I(\boldsymbol{r};\boldsymbol{R}(t+\Delta t))$. This is not an easy procedure since the ordering (according to the magnitude of the orbital energies) of molecular orbitals making up $\Phi_I(\boldsymbol{r};\boldsymbol{R}(t))$ frequently changes from time to time, and we easily lose the smooth connection between $\Phi_I(\boldsymbol{r};\boldsymbol{R}(t))$ and $\Phi_I(\boldsymbol{r};\boldsymbol{R}(t+\Delta t))$. Once the smooth one-to-one connection is lost, the mixing procedure among the electronic configurations in Eq. (5) becomes no longer correct, and tracking of the dynamics is destroyed. There are several ways to maintain the smooth one-to-one connection. In the present computation, the correspondence of the indexes of the set of molecular orbitals at one time step and of the set of molecular orbitals at an adjacent time step is

© Author(s) 2019

京都大学 KYOTO UNIVERSITY
A Self-archived copy in
Kyoto University Research Information Repository
https://repository.kulib.kyoto-u.ac.jp
京都大学学術情報リポジトリ KURENAI 紅 Kyoto University Research Information Repository

figured out by reordering one set of the molecular orbitals so that the overlap matrix between the two sets of molecular orbitals become nearly diagonal, assuming the molecular orbitals undergo only small change in the short time step. Then, we may regard that the CSFs built from similarly ordered molecular orbitals should correspond, and the CSF expansion coefficients are carried forward to the new set of CSFs.

Once the nonadiabatic trajectory $\boldsymbol{R}(t)$ and associated electronic expansion coefficients $\boldsymbol{C}(t)$ are obtained, observables such as the nuclear kinetic energy $T_{\mathrm{N}}(t)$,

$$T_{\mathrm{N}} = \sum_{k=1}^{3N} \frac{P_k^2(t)}{2m_k}, \tag{10}$$

and nuclear potential energy $V(t)$,

$$V(t) = \sum_I \sum_J C_I^*(t) H_{IJ}^{(\mathrm{el})}(\boldsymbol{R}(t)) C_J(t), \tag{11}$$

can be computed with the total energy being $E(t) = T_{\mathrm{N}}(t) + V(t)$, which is to be conserved.

The *ab initio* quantum chemistry package GAMESS[66] was used in obtaining the molecular orbitals and the CSF Hamiltonian $H_{IJ}^{(\mathrm{el})}(\boldsymbol{R}(t))$ at each set of nuclear coordinates $\boldsymbol{R}(t)$. The spatial derivatives in Eqs. (3) and (7) were evaluated by finite differencing between additionally computed nearby points. In addition to the nonadiabatic dynamics computed above, we show below the result of adiabatic dynamics for comparison. In that case, the electronic state is represented in a single adiabatic electronic state (obtained from diagonalization of the CSF Hamiltonian) at each set of nuclear coordinates $\boldsymbol{R}(t)$, whose time evolution reduces to

$$m_k \ddot{R}_k(t) = -\frac{\partial V(\boldsymbol{R}(t))}{\partial R_k}, \tag{12}$$

where $V(\boldsymbol{R}(t))$ is the adiabatic potential energy of the electronic state under question.

In Sec. III A, we use a procedure similar to adiabatic time evolution in quenching a state to a local minimum. Quenching is affected by resetting the momentum to zero before each time step, using only the force from the potential energy surface at each geometry to drive the molecule. Of course, "time" loses its physical sense in this case.

B. Physical properties used for analyses

In the rest of the paper, we make use of several quantities in analyzing aspects of the dynamics. The electronic energy components, atomic charge density, and, in particular, the unpaired electron density are found to be useful.

The electronic energy V is composed of several components,

$$V = T_{\mathrm{e}} + V_{\mathrm{e}}, \qquad V_{\mathrm{e}} = V_{\mathrm{ne}} + V_{\mathrm{ee}} + V_{\mathrm{nn}}, \tag{13}$$

where T_{e} is the electron kinetic energy, V_{e} is the electron potential energy, and V_{ne}, V_{ee}, and V_{nn} are, respectively, the energies of nuclear-electron attraction, electron-electron repulsion, and the nuclear-nuclear repulsion.

As an indicator for the electron distribution to stay in the interatomic bonding area, we first use the standard quantities extracted from the charge density. The atomic charge density matrix elements ρ_{AB},

$$\rho_{AB} = \sum_{\mu=1}^{N_{\mathrm{AO}}^{(A)}} \sum_{\nu=1}^{N_{\mathrm{AO}}^{(B)}} P_{\mu\nu}^{(AB)} S_{\mu\nu}^{(AB)}, \tag{14}$$

can aid in identifying the bonding structures in the time-evolving B_{12} cluster, where $N_{\mathrm{AO}}^{(A)}$ is the number of atomic basis functions centered on nucleus A, $S_{\mu\nu}^{(AB)}$ is the overlap matrix element between the real atomic basis functions $\chi_{A\mu}$ and $\chi_{B\nu}$, respectively, centered on nuclei A and B, and $P_{\mu\nu}^{(AB)}$ is the element of the density matrix in the atomic basis. The number of electrons n (equal to 60 for B_{12}) is the sum of the charge density matrix elements, consisting of a sum of the diagonal matrix elements n^{D} and a sum of the off-diagonal matrix elements n^{O},

$$n = n^{\mathrm{D}} + n^{\mathrm{O}}, \qquad n^{\mathrm{D}} = \sum_{A=1}^{N} \rho_{AA}, \qquad n^{\mathrm{O}} = 2\sum_{A=1}^{N} \sum_{B=1}^{A-1} \rho_{AB}. \tag{15}$$

To further characterize the chemical bonding of the highly excited states of the B_{12} cluster, we consider the unpaired electron density in addition to the charge density ρ_{AB}. The unpaired electron density is defined as[67]

$$\begin{aligned} D(\boldsymbol{r}) &= 2\rho(\boldsymbol{r},\boldsymbol{r}) - \int d\boldsymbol{r}' \rho(\boldsymbol{r},\boldsymbol{r}')\rho(\boldsymbol{r}',\boldsymbol{r}) \\ &= \sum_{i=1}^{N_{\mathrm{MO}}} n_i(2-n_i)\lambda_i^*(\boldsymbol{r})\lambda_i(\boldsymbol{r}), \end{aligned} \tag{16}$$

where $\rho(\boldsymbol{r}, \boldsymbol{r}')$ is the first-order reduced density matrix and the set $\{\lambda_i(\boldsymbol{r})\}$ is of the natural orbitals with $\{n_i\}$ their occupation numbers obtained by diagonalizing the reduced density matrix. N_{MO} is the number of molecular orbitals, which is the same as the number of natural orbitals. The unpaired electron number u is given by the trace

$$u = \int D(\boldsymbol{r}) d\boldsymbol{r}. \tag{17}$$

A natural orbital $\lambda_i(\boldsymbol{r})$ is a linear combination of the real atomic basis functions $\{\chi_{A\mu}(\boldsymbol{r})\}$, each centered on the nuclei indexed with A as

$$\lambda_i(\boldsymbol{r}) = \sum_{A=1}^{N} \sum_{\mu=1}^{N_{\mathrm{AO}}^{(A)}} C_{A\mu}^i \chi_{A\mu}(\boldsymbol{r}), \tag{18}$$

with the expansion coefficients $\{C_{A\mu}^i\}$. The unpaired electron density may be represented in the atomic basis,

$$D_{AB}(\boldsymbol{r}) = \sum_{i=1}^{N_{\mathrm{MO}}} \sum_{\mu=1}^{N_{\mathrm{AO}}^{(A)}} \sum_{\nu=1}^{N_{\mathrm{AO}}^{(B)}} n_i(2-n_i) C_{A\mu}^{i*} C_{B\nu}^i \chi_{A\mu}(\boldsymbol{r}) \chi_{B\nu}(\boldsymbol{r}), \tag{19}$$

and the unpaired electron density $D(\boldsymbol{r})$ may be thought to consist of a diagonal component $D^{\mathrm{D}}(\boldsymbol{r})$ and an off-diagonal component $D^{\mathrm{O}}(\boldsymbol{r})$,

$$D(\boldsymbol{r}) = D^{\mathrm{D}}(\boldsymbol{r}) + D^{\mathrm{O}}(\boldsymbol{r}), \tag{20}$$

with

$$D^{\mathrm{D}}(\boldsymbol{r}) = \sum_{A=1}^{N} D_{AA}(\boldsymbol{r}), \qquad D^{\mathrm{O}}(\boldsymbol{r}) = 2\mathrm{Re}\sum_{A=1}^{N} \sum_{B=1}^{A-1} D_{AB}(\boldsymbol{r}). \tag{21}$$

© Author(s) 2019

京都大学 KYOTO UNIVERSITY
A Self-archived copy in
Kyoto University Research Information Repository
https://repository.kulib.kyoto-u.ac.jp
京都大学学術情報リポジトリ KURENAI 紅 Kyoto University Research Information Repository

The unpaired electron density may be represented also as a matrix of atomic unpaired electron density D_{AB} by integrating over the electron coordinates,

$$D_{AB} = \int D_{AB}(\boldsymbol{r})d\boldsymbol{r}. \tag{22}$$

Then, analogous to the electron number from the charge density in Eq. (15), the unpaired electron number u is also made up of a diagonal component u^{D} and an off-diagonal component u^{O} such that

$$u = u^{\mathrm{D}} + u^{\mathrm{O}}, \qquad u^{\mathrm{D}} = \sum_{A=1}^{N} D_{AA}, \qquad u^{\mathrm{O}} = 2\mathrm{Re}\sum_{A=1}^{N}\sum_{B=1}^{A-1} D_{AB}. \tag{23}$$

III. FEATURES OF THE STATIC ELECTRONIC STATES

A. Potential-basin structures

Before considering the time-evolving chemical bonding seen in the dynamics of highly electronically excited boron clusters, we call attention to the rather unusual nature of these excited states as background. We first take a quick look at the excited states of the B_2 molecule as an easily visualized example of densely quasi-degenerate set of excited states, followed by examples of similar local minima on diverse excited states of the B_{12} clusters, suggesting that the dynamics is not determined by properties of the individual excited states. Then in Sec. III B, we demonstrate the frequent occurrence of conical intersections and avoided crossings along the excited state trajectory. Such frequent nonadiabatic interaction, also clearly shown in Figs. 11–13 in the previous paper,[44] is an essential property of the nonadiabatic trajectory in densely quasi-degenerate electronic states.

Figure 1 shows the ground and excited potential energy curves of the B_2 molecule. A minimum Slater-type orbital (STO)-3G basis set is used, but a configuration interaction (CI) of 6 electrons distributed in 8 orbitals (all except the atomic 1s orbitals; excitation not restricted to singles and doubles only) results in 1176 states. All 1176 states are drawn in Fig. 1. Since a boron atom has the ground-state configuration as $[1s^2, 2s^2, 2p^1]$, it is readily expected that even the diatomic molecule B_2 should have many excited states of bound nature. Indeed, Fig. 1 shows many bound states and predissociating states high above the ground state. The ground state is in fact a spin-triplet having the configuration $[1\sigma_g^2, 1\sigma_u^2, 2\sigma_g^2, 2\sigma_u^2, 1\pi_u^1, 1\pi_u^1]$. Figure 1 would have been more complicated had triplet states been included, but we limit the present study to the spin-singlet states

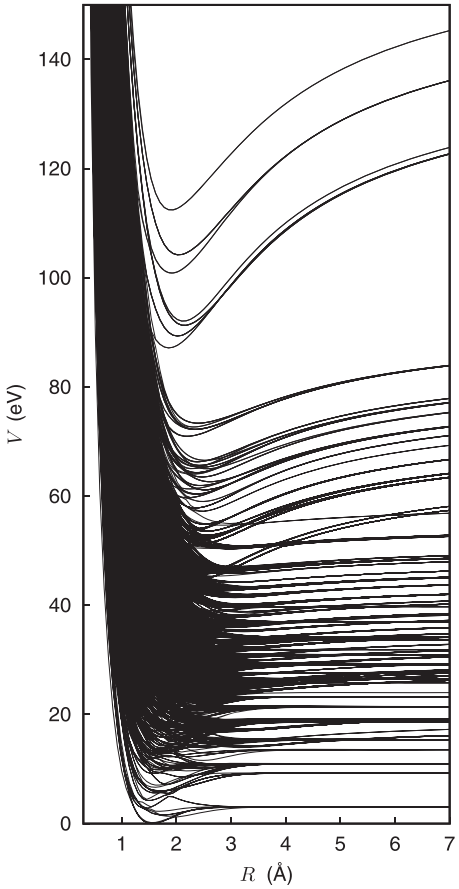

FIG. 1. Singlet adiabatic potential energy curves of the B_2 molecule. Configuration interaction of 6 electrons in 8 orbitals with the STO-3G basis set.

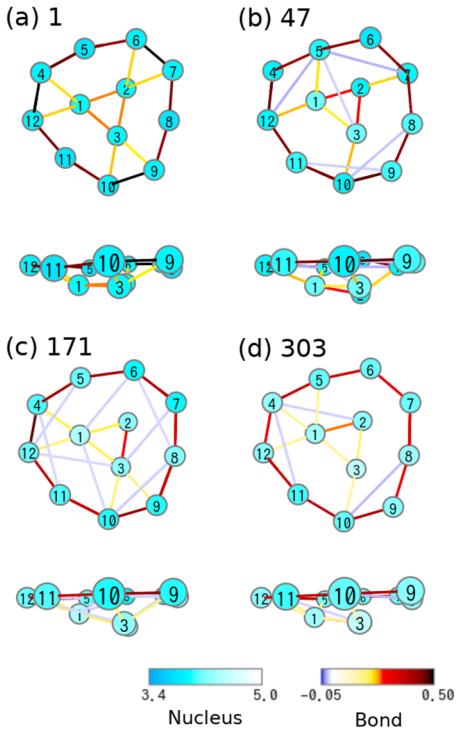

FIG. 2. Structures reached by quenching down to a (possibly local) potential minimum on the adiabatic states (a) 1, (b) 47, (c) 171, and (d) 303. Each structure is seen from two different directions. Balls and sticks representing nuclei and bonds, respectively, are colored according to their ρ_{AA} (electron density on each atom) and ρ_{AB} values (that in the inter-atomic region), the details of which are defined in Eq. (14) and in the caption of Fig. 9. The color bar indicated by nucleus (bond) is applied to the value of ρ_{AA} (ρ_{AB}).

© Author(s) 2019

京都大学 KYOTO UNIVERSITY
A Self-archived copy in
Kyoto University Research Information Repository
https://repository.kulib.kyoto-u.ac.jp
京都大学学術情報リポジトリ KURENAI 紅 Kyoto University Research Information Repository

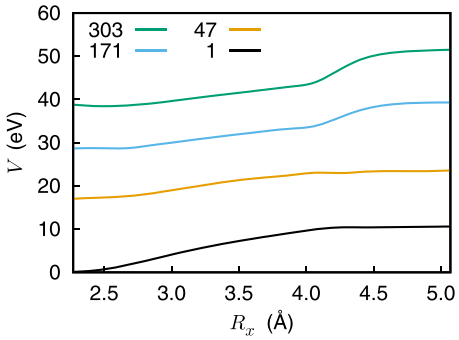

FIG. 3. Adiabatic energy curves along an arbitrary dissociation direction. The R_x coordinate of a peripheral nucleus is varied.

(also in the B_{12} study). In the linear and symmetric B_2 molecule, only states belonging to the same spatial irreducible representation interact with each other, but we note that for larger molecules such as B_{12} undergoing dynamics, such a symmetry will not in general exist.

If we imagine the diabatic energy curves that result in the pictured adiabatic energy curves, we can see that there are diabatically dissociating states. But we also see that the dissociating diabatic states invariably cross one or more bound diabatic states so that there are no purely dissociating adiabatic states (again, in the B_2 molecule, symmetry considerations might say otherwise). There will be numerous intersections and local minima within a few angstroms of each atom's movement in the excited states of the B_{12} cluster.

Thus, we expect each of the excited states of B_{12} to have minima (not necessarily global ones), for example, not far from the global minimum geometry of the ground electronic state. Figure 2 shows the geometries reached by quenching near the global minimum geometry on the adiabatic states 1 (the ground state), 47, 171, and 303. The quenched minimum geometries are all close to the global minimum geometry on state 1, in which there are 9 peripheral atoms positioned with a 120° orientational symmetry nearly in a plane. The inner 3 atoms are not in the same plane as the outer atoms. The inner atoms' plane is parallel to the outer atoms' plane for the ground electronic state but not necessarily so for the excited states. These molecular structures and chemical bonds provide us with the quantum chemical understanding of the static boron. However, the goal of this paper is not to analyze the nature of chemical bonds at these local minima.[68] Besides, these local minimum states are practically inaccessible because the electronic-nuclear states encounter so many nonadiabatic transitions before reaching the bottoms of the potential basins.

To show explicitly that the local minima thus found have ascending slopes toward the dissociation directions, we show in Fig. 3 the potential curves along an arbitrary dissociation direction. The R_x coordinate of a peripheral nucleus, the one with the largest R_x value, is varied from its initial position (2.27 Å) toward a larger value, while all other coordinates are fixed with no geometrical optimization. The states 1, 171, and 303 shown have dissociation energies exceeding 10 eV in this direction. State 47 has a dissociation height in this direction of 6.6 eV. Had the bound part of the cluster left behind by the dissociating nucleus been relaxed in energy, the dissociation barriers would have been lower. The trajectory computations given in Secs. III B and IV were started with an initial kinetic energy of 7.2 eV and an additional initial potential energy as stated in Sec. IV A, significantly higher than the dissociation energies. Later in Sec. V B, when we focus on the effect on dissociation of the quasi-degenerate states of the B_{12} cluster, even higher energies are considered for the trajectories.

B. Frequent encounter with conical intersections and avoided crossings

Figure 4 shows the adiabatic energy (black curves) along adiabatic trajectories [adiabatic state 10 in Fig. 4(a) and adiabatic state 303 in Fig. 4(b)]. Although each adiabatic trajectory stays in the same adiabatic state throughout the time evolution by definition, we see frequent encounters with conical intersections and nearly avoided encounters with conical intersections in the adiabatic energy evolution. In Fig. 4(a), arrows point out an example of each kind. At higher states [Fig. 4(b)], the neighboring adiabatic energies are quite close to each other, indicating a very high quasi-degeneracy, which should increase the importance of taking full account of nonadiabatic interactions.

IV. DYNAMICAL CHEMICAL BONDING IN BORON CLUSTERS

We here track the real-time nonadiabatic electron dynamics aiming at the extraction of the essential feature of the dynamical chemical bonding. In Sec. IV B, we see that the dynamics of the electronic energy is related to the fluctuation of chemical bonding and, in particular, that the nonadiabatic mixed nature of highly excited states is reflected in the deviation of the virial ratio from 2. The time-evolving bonding structure, seen through the atomic charge distributions, can be simply summarized with the notion of

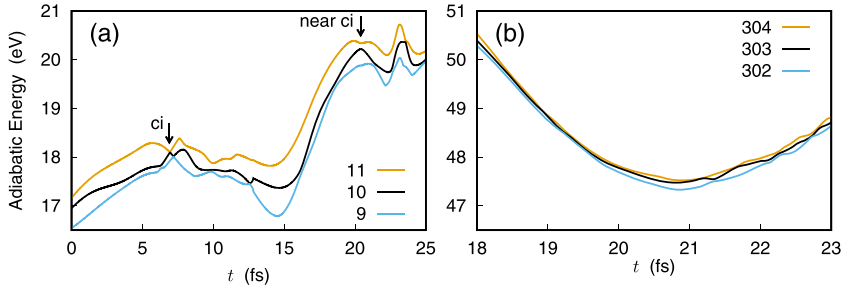

FIG. 4. Adiabatic potential energy along the adiabatic trajectory (a) on state 10 and (b) state 303. Adiabatic potential energy of states one above and below the state used for the trajectories is also shown. In (a), arrows point out an encounter with a conical intersection (ci) and a near encounter.

© Author(s) 2019

京都大学 KYOTO UNIVERSITY
A Self-archived copy in
Kyoto University Research Information Repository
https://repository.kulib.kyoto-u.ac.jp
京都大学学術情報リポジトリ KURENAI 紅 Kyoto University Research Information Repository

"string and web" and their dynamical reconnection, as discussed in Sec. IV C. Then, in Sec. IV D, we see that negative unpaired electron distribution is characteristically seen in the inter-atomic bonding areas in the highly excited states and discuss its role.

A. Initial conditions for nonadiabatic electron dynamics

All the numerical presentations made below are based on the full electron wavepacket and nuclear *ab initio* dynamics calculations. However, since we do not aim to obtain numerically accurate results in this paper, and since the size of numerical computation could become very large, our study is limited to be qualitative or at most semiquantitative. To keep the computation tractable, the electronic state of the B_{12} cluster is represented in the STO-3G minimum basis set[69] and the set of configuration state functions is obtained by excitation of the two highest-occupied molecular orbital (HOMO) electrons into all the virtual orbitals, restricted to the singlet configurations. The number of CSFs is $N_{CSF} = 496$. Exciting from only the HOMO is justified in that the orbital energy of the HOMO does not come close to that of the orbital one below it (HOMO − 1) during the time evolution (see the supplementary material). HOMO − 1 does approach in energy to orbitals below it. We think the minimum representation of the excited states of B_{12} all the more captures the qualitative features of the very complicated electron dynamics expected in the densely quasi-degenerate states. A larger basis set and/or a larger configuration space will only increase more complexity and not mar the qualitative conclusions to be drawn here.

Two sets of dynamics computations are presented in the following sections (one set in Sec. IV and a second in Sec. V B). In one set, the initial geometry of the B_{12} cluster is taken to be the global minimum of the ground electronic state, modified by adding arbitrarily ±0.08 Å to each coordinate (resulting in the CI ground state energy to be above the global minimum by 4.9 eV). An initial kinetic energy of 0.2 eV is given to each coordinate direction (momentum is positive or negative arbitrarily) for a total of 7.2 eV in kinetic energy. The translational momentum and the total angular momentum are adjusted to zero. A single adiabatic state is chosen as the initial electronic state. Thus, the initial energy is much higher than the dissociation threshold (see Sec. III A) though the nonadiabatic trajectories of the cluster remain bound for at least the 200 fs computed. All trajectories are computed with a time step Δt of 0.01 fs.

We first prepare a set of sampling SET paths, with which to show the present performance of the smooth one-to-one connection among the CSF basis functions in the SET calculations. These paths are also adopted for the analyses of complexity of the dynamical electronic states in what follows. Figure 5 shows the time evolution of difference energies for four nonadiabatic trajectories, each started from the pure adiabatic state 1, 2, 44, and 282, with initial potential energies of 4.948 eV, 8.399 eV, 20.741 eV, and 42.991 eV, respectively, as examples of nonadiabatic trajectories with low, middle, and high total energies. The orange curves show the time evolution of the potential energy as the difference from the initial potential energy ($V(t) - V(0)$), and the black curves show the kinetic energy as the negative of the difference from the initial kinetic energy. The discrepancy between the orange and the black curves indicates error in the total energy. The blue curves show the total energy as the difference from the initial energy. In several places, we see a deviation to some extent exist between the nuclear potential energy and the nuclear kinetic energy. In particular, the initial state 282 trajectory encounters so large an error at $t = 176$ [Fig. 5(d)] that we gave up keeping track of it at this time. At such time steps, the set of molecular orbitals obtained at one time step and at an adjacent time step differs significantly. The self-consistent-field electronic state calculations at adjacent time steps converge to a noncorresponding set of molecular orbitals. The simple assignment procedure used for the continuity of CSFs given in Sec. II A breaks down at these points. The smooth one-to-one connection among the CSF

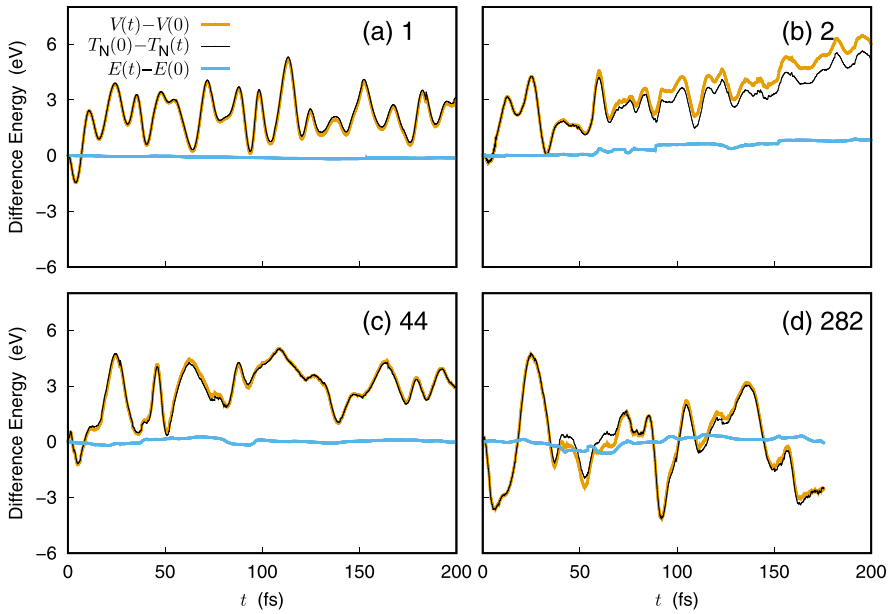

FIG. 5. Time evolution of difference energies along nonadiabatic trajectories started from pure adiabatic states (a) 1, (b) 2, (c) 44, and (d) 282.

© Author(s) 2019

京都大学 KYOTO UNIVERSITY
A Self-archived copy in
Kyoto University Research Information Repository
https://repository.kulib.kyoto-u.ac.jp
京都大学学術情報リポジトリ KURENAI 紅 Kyoto University Research Information Repository

basis functions can be that difficult in treating those heavily quasi-degenerate states. Nonetheless, we also see that apart from the few discontinuous points, the total energy is mostly well conserved (the correspondence of CSFs between adjacent time steps is recovered after a discontinuity, though the trajectory afterwards has a slightly different total energy). Those SET paths driven in the densely quasi-degenerate electronic manifold are readily conceived to be embedded in a chaotic sea. As an analogy, we recall the shadowing lemma in chaos theory,[70] which is nicely digested by Guckenheimer and Holmes as "While a computer may not calculate the orbit which you hope for, what it does find is nonetheless an approximation to some true orbit of the system."[71]

In another set of dynamics computations, we generate a set of nuclear coordinates and momentum that would result in dissociation in an adiabatic time evolution and compare the adiabatic and nonadiabatic trajectories as detailed in Sec. V B.

B. Dynamics and energetics of electronic states

We first survey the interrelation behind the electronic energy and chemical bonding. Figure 6 displays the time variation of the total one-particle energy of the electrons, $T_e + V_{ne}$ (orange curves), and the total of the two-particle energy, the electron-electron repulsion energy, V_{ee} (blue curves, shifted down $-1500\ E_h$ to use the same scale as the one-particle energy), along with the number of electrons in the off-diagonal elements or the off-diagonal electron number n^O. The panels (a)–(d) show the cases for nonadiabatic trajectories starting from the adiabatic states 1 (the ground state), 2, 44, and 282, respectively. It is immediately seen that for the low energy cases up to the 44th, the electronic repulsion energy V_{ee} varies in-phase with n^O, while the one-electron energy, which corresponds to the transfer integral or the resonance energy in the Hückel theory, evolves out-of-phase with n^O. V_{ee} behaves naturally out-of-phase with $T_e + V_{ne}$. The covalent type of chemical bonds should be generally enhanced by the lowering of the one-electron integral,[68] which in turn push the electrons to the inter-atomic regions. On the other hand, the electron-repulsion energy seems to be accumulated in the inter-atomic energy as the chemical bond becomes more prominent. (Incidentally, we recall that the Hubbard Hamiltonian[72] presupposes that the electron repulsion energy is raised as the atomic-site electronic population increases. Therefore, the behavior seen in Fig. 6 is rather counter intuitive.) Very interestingly, the dynamical interrelation between n^O and both $T_e + V_{ne}$ and V_{ee} tends to fade away for higher energies, although the out-of-phase relationship between $T_e + V_{ne}$ and V_{ee} remains with a large fluctuation both in magnitudes and time of oscillation. The former fact seems to suggest that n^O alone is not necessarily a good quantity any longer to measure the extent of chemical bonding.

Figure 7(a) shows the time evolution of the electron kinetic energy T_e along the nonadiabatic trajectories starting from the adiabatic states 1, 2, 44, and 282, while Fig. 7(b) shows the time evolution of the electron potential energy $V_e = V_{ne} + V_{ee} + V_{nn}$ along the same trajectories. Figure 7(c) shows the virial ratio $-V_e/T_e$, which should be 2 for the exact Born–Oppenheimer adiabatic electronic wavefunctions. We see, as expected, that at $t = 0$ (where initially the trajectories start from an adiabatic state), the ground state virial ratio is 1.987 for the present minimum basis set CI calculation. Recall that the virial ratio of 2 is a direct consequence from a scaling law inherent in the (static) Coulombic field the electrons are placed in. Yet, the nuclear kinematic coupling as the nonadiabatic interaction generally breaks this scaling property and allows the virial ratio $-V_e/T_e$ to deviate from 2. Our numerical calculations have shown that the ratio of the magnitudes of nonadiabatic couplings to that of the electronic Hamiltonian is larger for the higher excited states, and the deviation from the virial theorem becomes more evident as seen in panel (c) of Fig. 7. It is also seen that the virial ratio oscillates to some extent along the nonadiabatic time evolution. The smaller virial ratio seen in the higher electronic energy states implies that T_e and/or

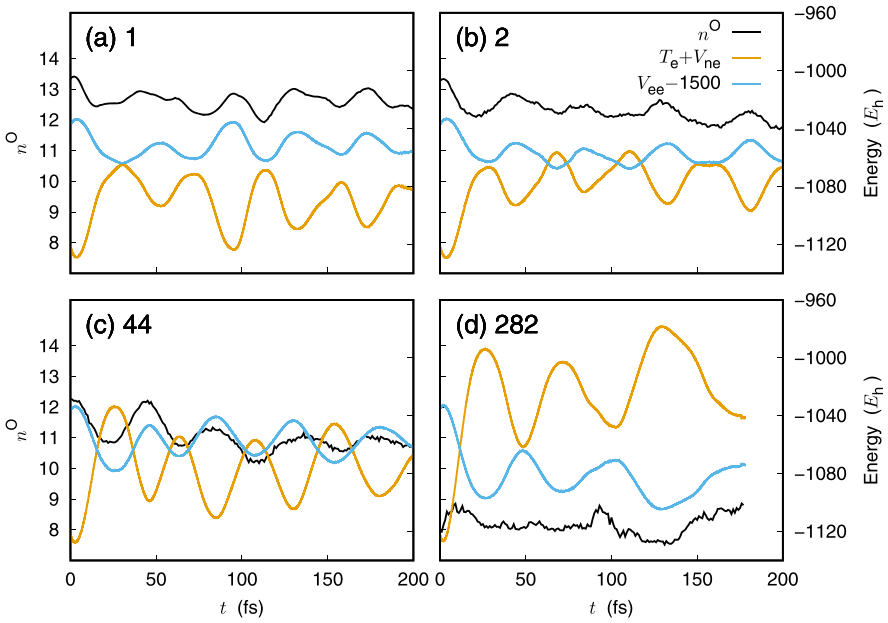

FIG. 6. Off-diagonal electron numbers n^O (black curves), the one electron energy $T_e + V_{ne}$ (orange curves), and the electron-electron repulsion energy V_{ee} (blue curves, shifted down by $-1500\ E_h$ for ease of comparison with the other curves) along the nonadiabatic trajectories starting from adiabatic states (a) 1, (b) 2, (c) 44, and (d) 282.

© Author(s) 2019

京都大学 KYOTO UNIVERSITY
A Self-archived copy in
Kyoto University Research Information Repository
https://repository.kulib.kyoto-u.ac.jp
京都大学学術情報リポジトリ KURENAI 紅 Kyoto University Research Information Repository

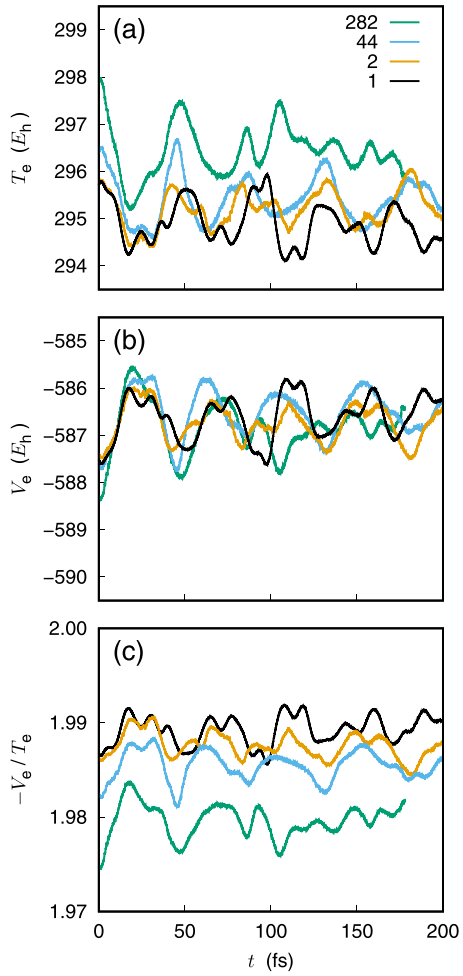

FIG. 7. Time evolution of (a) electron kinetic energy T_e, (b) electron potential energy $V_e = V_{ne} + V_{ee} + V_{nn}$, and (c) virial ratio $-V_e/T_e$ along nonadiabatic trajectories starting from the adiabatic states 1, 2, 44, and 282.

V_{ne} become larger (smaller absolute magnitude for V_{ne}) for the higher excited states. This is understandable since the nonadiabatic interaction works as a kinematic coupling like "friction" between electrons and nuclei and should suppress the Born–Oppenheimer assumption that the electronic wave can instantaneously adjust to the nuclear motion. Hence, the electronic wavefunction cannot be located at the best place with respect to the nuclear configuration. The electronic kinetic energy thus attained is likely to be utilized for the electronic mobility so as to wander from one adiabatic state to another.

Incidentally, the relevance or irrelevance of the virial theorem in the nature of chemical bond has been discussed very recently by Bacskay, Nordholm, and Ruedenberg[73] (see also Ref. 68). The present work reveals that the deviation from the virial theorem in the energy of electrons placed in a molecular Coulombic field is a physical manifestation of the kinematic coupling between nuclei and electrons. It thus highlights that the chemical bonding studied here is essentially different from the static chemical bonds. As another clear-cut example of physical manifestation of the nonadiabatic interactions, the correlation function between electronic flux and nuclear flux has been extensively studied.[74,75]

C. String and web in chemical bonding

For further analyses of the nature of the present chemical bonding, we show in Fig. 8 examples of the atomic charge density matrix (elements ρ_{AB}) and atomic unpaired electron density matrix (elements D_{AB}) for the global minimum geometry of the adiabatic ground state [Fig. 8(a)] and for geometries along the nonadiabatic trajectories starting from the adiabatic states 44 and 282, respectively [Figs. 8(b) and 8(c)]. The atomic charge density matrix is symmetric, and only the upper triangle including the diagonal is shown for each panel. The atomic unpaired electron density matrix is Hermitian, and only the real part of it is shown as the lower triangle including the diagonal in each panel. Table I summarizes the electron numbers and unpaired electron numbers obtained as the sum of the matrix elements given in Fig. 8.

The atomic unpaired electron density matrix is further discussed later in Sec. IV D. For now, we focus on the atomic charge density matrix in this subsection. In Fig. 8(a), the atomic charge density matrix at the global minimum geometry of the ground electronic state [see Fig. 2(a)] is shown. On the diagonal, we see that ~4 electrons are bound to each nucleus. The off-diagonal elements suggest that most interatomic charge densities are zero or slightly negative, but between some atoms, there are moderate ($0.21 \le \rho_{AB} \le 0.23$) or strong ($0.44 \le \rho_{AB} \le 0.51$) elements, indicating interatomic bonds. We note that the strong bonds are between the 9 peripheral atoms, forming a ring. The global minimum geometry belongs to the C_{3v} point group, and the atomic charge density matrix shows the corresponding symmetry.

Figure 8(b) shows the atomic charge density matrix for a higher energy (at a nuclear geometry 50 fs after starting a nonadiabatic trajectory from the adiabatic state 44). Figure 8(c) shows the case at an even higher energy (at a nuclear geometry 130 fs after starting a nonadiabatic trajectory from the adiabatic state 282). The diagonal elements are larger as the energy is increased (see also Table I), and the off-diagonal elements are correspondingly smaller.

Figure 9 shows typical bonding structures found along the nonadiabatic trajectory starting from the adiabatic electronic state 282. Bonds corresponding to the atomic charge density value $\rho_{AB} \ge 0.25$ are colored red. We see that there are mostly up to two such strong bonds per atom, imposing a string-like structure involving some of the atoms, where the other atoms attach loosely [$\rho_{AB} < 0.25$, yellow bonds in Fig. 9(a)]. We can call the bonding structure made up of the stronger bonds the "main string," to which other atoms are loosely attached in a "web." Sometimes the main string is actually a ring as in the 5 fs example of Fig. 9. Panel (b) shows a symbolic representation of the string structures by connecting the atom numbers committing directly to the strings. The brackets [ ] indicate a ring shape of the string. Sometimes the main string is made up of several strings as in the 40 and 130 fs examples. These string structures aid in classifying the bonding structure and its evolution along the trajectory, characterizing bond breaking and reconnections. Dynamics and precise mechanism of reconnection will be discussed in future papers.

© Author(s) 2019

京都大学 KYOTO UNIVERSITY
A Self-archived copy in
Kyoto University Research Information Repository
https://repository.kulib.kyoto-u.ac.jp
京都大学学術情報リポジトリ KURENAI 紅 Kyoto University Research Information Repository

(a)

Atomic charge density matrix

	12	4	5	6	7	8	9	10	11	3	1	2	
	3.90	0.51	-0.02						0.44	-0.02	0.21		12
		3.90	0.44						-0.02		0.21	-0.02	4
12	0.02		3.81	0.44	-0.02					-0.02			5
4		0.02		3.90	0.51	-0.02					-0.02	0.21	6
5			0.01		3.90	0.44				-0.02		0.21	7
6				0.01		3.81	0.44	-0.02			-0.02		8
7					0.01		3.90	0.51	-0.02	0.21		-0.02	9
8						0.01		3.91	0.44	0.21	-0.02		10
9							0.01		3.81			-0.02	11
10								0.01		3.97	0.23	0.23	3
11									0.01		3.97	0.23	1
3										0.01		3.97	2
1											0.01		
2												0.01	

Atomic unpaired electron density matrix

(b)

Atomic charge density matrix

	9	10	11	12	4	5	6	7	8	3	2	1	
	4.00	0.53	-0.01							0.37	-0.02		9
		3.88	0.47	-0.01					-0.01				10
9	0.32		3.92	0.44									11
10	-0.05	0.50		4.09	0.44	-0.02				-0.01	-0.01	0.27	12
11			0.50		4.09	0.42					-0.03		4
12			-0.05	0.47		3.99	0.49	-0.01		-0.01			5
4				-0.06	0.42		3.90	0.48	-0.02	-0.01		-0.01	6
5					-0.04	0.41		4.08	0.42	-0.02			7
6						-0.04	0.32		4.10	0.29		-0.01	8
7								0.45		4.02	0.31		3
8	-0.05	0.01						-0.06	0.46		4.01	0.35	2
3		-0.06							-0.05	0.47		4.00	1
2					-0.02	-0.04		-0.03	-0.03	-0.05	0.44		
1				-0.05	-0.04	-0.04						0.52	

Atomic unpaired electron density matrix

(c)

Atomic charge density matrix

	6	2	8	9	12	4	5	1	11	10	3	7	
	4.34	0.28	-0.01			-0.01	0.20					0.15	6
		4.28	*0.35	-0.01			-0.01						2
6	0.52		4.41	0.30					-0.01				8
2	-0.09	0.72		4.46						0.13			9
8		-0.20	0.76		4.32	0.28	-0.02		0.24	-0.01			12
9			-0.14	0.51		4.40	0.34		-0.02				4
12					0.50		4.21	0.31					5
4					-0.11	0.52		4.36	0.33	-0.01			1
5	-0.05					-0.04	0.51		4.15	0.31			11
1						-0.08	-0.15	0.74		4.32	0.21		10
11					-0.06			-0.17	0.68		4.50		3
10									-0.13	0.58		4.63	7
3		-0.06	-0.08	0.01						-0.12	0.59		
7												0.34	

Atomic unpaired electron density matrix

FIG. 8. Examples of atomic charge density matrix (the upper triangle) and the real part of atomic unpaired electron density matrix (the lower triangle) at (a) the global minimum geometry of the adiabatic ground state. (b) The same for the geometry along the nonadiabatic trajectory 50 fs after starting from adiabatic state 44 and (c) 130 fs after starting from adiabatic state 282. Numbers along the edges identify the atomic nuclei. Values within (−0.01, 0.01) are not shown.

© Author(s) 2019

京都大学 KYOTO UNIVERSITY
A Self-archived copy in
Kyoto University Research Information Repository
https://repository.kulib.kyoto-u.ac.jp
京都大学学術情報リポジトリ KURENAI 紅 Kyoto University Research Information Repository

TABLE I. Electron numbers and unpaired electron numbers for the matrices given in Fig. 8.

Initial state	n^{D}	n^{O}	u	u^{D}	u^{O}
1	46.76	13.24	0.12	0.13	−0.01
44	48.09	11.91	3.53	5.28	−1.75
282	52.38	7.62	3.76	6.96	−3.20

D. Negative unpaired electron density in the bonding region

1. Characteristic distribution of the negative unpaired electron density

The lower triangle of each panel of Fig. 8 shows the real part of elements of the atomic unpaired electron density matrix D_{AB}, Eq. (22). We see that for the ground adiabatic state [Fig. 8(a)], there are essentially no unpaired electrons except small numbers in the diagonals. For the matrix taken from the trajectory starting from the adiabatic state 44 [Fig. 8(b)], there is significant unpaired electron density in the diagonals (an average of 0.4). There is also negative unpaired electron density in the off-diagonals in this case, often along the main strings where the charge density in the bond is significant but not always. For the trajectory starting from an even higher adiabatic state 282 [Fig. 8(c)], both the positive diagonal unpaired electron density and the negative off-diagonal unpaired electron density have higher magnitudes than for the lower adiabatic states.

Figure 10(a) shows the off-diagonal part of the unpaired electron density $D^{O}(\boldsymbol{r})$, Eq. (21). Figures 10(b) and 10(c) show the unpaired electron numbers u [the orange curve, Eq. (23)] for each adiabatic state at the global minimum geometry of the adiabatic ground state. For this figure only, the active space for configuration interaction is taken to be single and double excitations from the HOMO − 1 and HOMO into all virtual orbitals of the ground state (four electrons). This was the active space in the previous paper,[44] and Fig. 10 can be compared directly with Fig. 8 (and Fig. 2) of that paper.[44]

The spatial distribution of the unpaired electron density, $D(\boldsymbol{r})$ in Eq. (16), and its components $D^{D}(\boldsymbol{r})$ and $D^{O}(\boldsymbol{r})$ in Eq. (21) are some of the few quantities that can clearly distinguish the adiabatic electronic states.[44] Figure 10(a) shows the off-diagonal unpaired electron density $D^{O}(\boldsymbol{r})$ for the adiabatic states 40 and 300. We see positive and negative unpaired electron density exhibit a certain pattern in $D^{O}(\boldsymbol{r})$ for the adiabatic state 40; such patterns were found to help distinguish quasi-degenerate adiabatic states in the previous work.[44] As can be clearly identified, $D^{O}(\boldsymbol{r})$ for the adiabatic state 300 is (slightly) positive in the bonding region, while negative density of a large intensity is seen in the inter-atomic areas. We may say that the off-diagonal component (i.e., not on the nuclei) is the number of unpaired electrons found in the bonding region or in the region between the nuclei, which increases for higher adiabatic states.

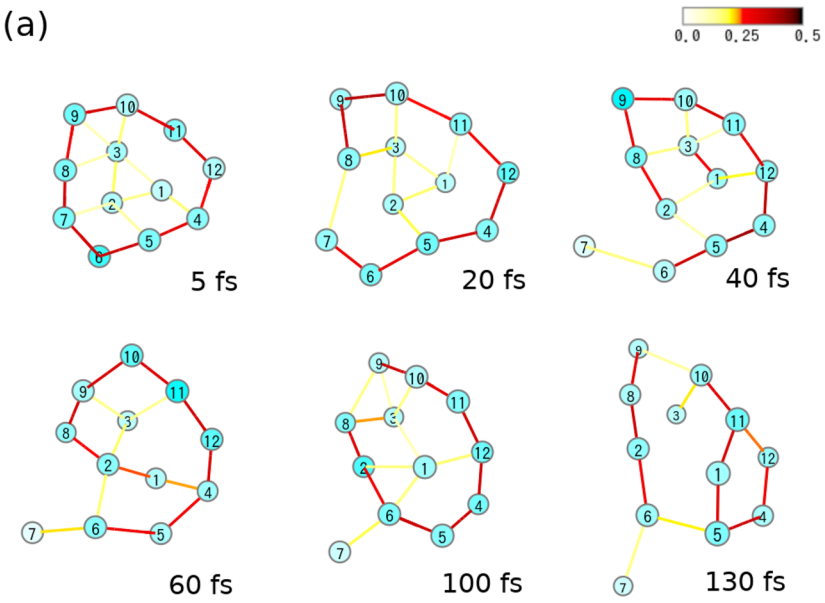

FIG. 9. Bonding structure along the nonadiabatic trajectory starting from the adiabatic state 282, at 5, 20, 40, 60, 100, and 130 fs after the start of the time evolution. (a) The spatial geometry is shown in a similar way to Fig. 2, where red bonds indicate the main string structure ($\rho_{AB} \geq 0.25$) and orange and yellow bonds indicate weaker attachments (color-bar shown at top right). Balls representing nuclei are colored as in Fig. 2. Note that the ends of bonds may be seen in front of nuclei or be hidden behind nuclei depending on relative nuclei depth. (b) The main string structures are summarized in a symbolic representation.

© Author(s) 2019

京都大学 KYOTO UNIVERSITY
A Self-archived copy in
Kyoto University Research Information Repository
https://repository.kulib.kyoto-u.ac.jp
京都大学学術情報リポジトリ KURENAI 紅 Kyoto University Research Information Repository

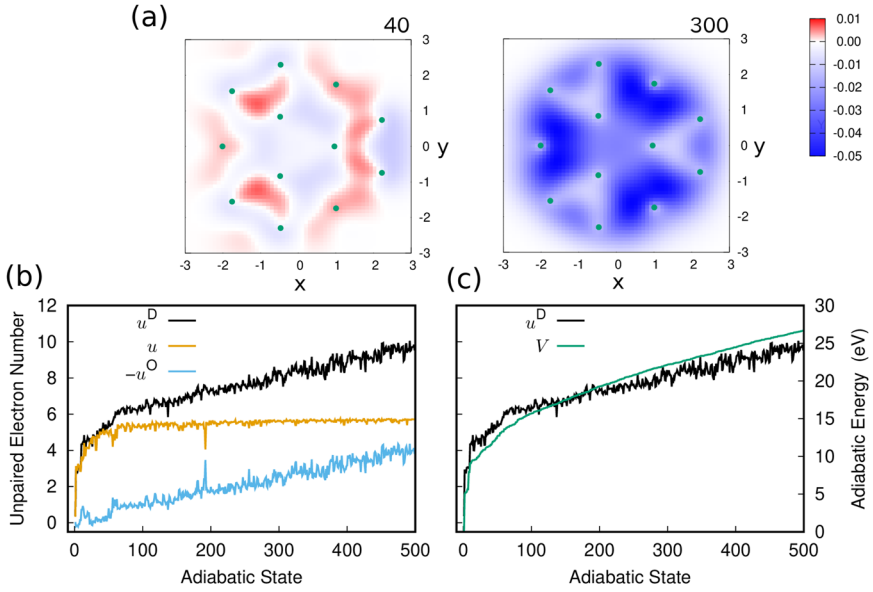

FIG. 10. (a) The off-diagonal part of the unpaired electron density $D^O(\boldsymbol{r})$ integrated over the z coordinate, seen in the xy-plane (parallel to the molecular ring) for the adiabatic states 40 and 300, at the global minimum geometry of B_{12}. Green dots indicate nucleus positions. (b) Unpaired electron numbers $u = u^D + u^O$, with the diagonal and off-diagonal components u^D and u^O, respectively, for each adiabatic state at the global minimum geometry. Note that negative u^O values are shown. (c) The adiabatic electronic energies V at the global minimum geometry, compared with the diagonal unpaired electron numbers u^D. In (b) and (c), lines connect discrete points to aid visibility.

To see a larger picture, we show Fig. 10(b), in which the unpaired electron numbers u (the orange curve) are broken into their components. The unpaired electron number u is a sum of a diagonal component u^D and an off-diagonal component u^O, shown as the black and blue curves, respectively, in Fig. 10(b). The diagonal component u^D was presented mistakenly as the total component u in Fig. 8 of the previous paper.[44] The unpaired electron number u increases from 0 to 5 for the adiabatic states 1 through 90 and for higher adiabatic states remain at 5. The components that make up u keep changing for states above 90, however. The diagonal component u^D [the black curve in Fig. 10(b)] keeps increasing in number up to state 500, with a corresponding decrease in the off-diagonal component u^O that keeps the total roughly constant [note that the negative of the off-diagonal component is plotted as the blue curve in Fig. 10(b)]. The increase in negative unpaired electron density in the bonding region, corresponding to the decrease in the off-diagonal unpaired electron number component, was seen in Fig. 8(c) of the previous paper.[44]

In Fig. 10(c), the diagonal component of the unpaired electron number u^D (the black curve) is compared with the adiabatic energies (the green curve), showing the rough correspondence of the slopes of the curves for differing regions of the energy and u^D.

2. Role of the negative unpaired electrons; strength and depth of chemical bonding

A physical consequence of the decrease in the negative unpaired electron density (the increase in the absolute value) in the interatomic regions can be conceived as follows. In the electron density,

$$\rho(\boldsymbol{r}) = \sum_i n_i \lambda_i^*(\boldsymbol{r})\lambda_i(\boldsymbol{r}), \tag{24}$$

and the unpaired electron density, $D(\boldsymbol{r})$ of Eq. (16),

$$D(\boldsymbol{r}) = \sum_i n_i(2-n_i)\lambda_i^*(\boldsymbol{r})\lambda_i(\boldsymbol{r}), \tag{25}$$

let us expand a single natural orbital $\lambda_i(\boldsymbol{r})$ in terms of real atomic orbitals (basis functions),

$$\lambda_i(\boldsymbol{r}) = \sum_A^{\mathrm{AO}} C_A^i \chi_A(\boldsymbol{r}). \tag{26}$$

Here, we simplify for clarity of the notation [of Eq. (18)] so that a summation over A of AO includes all the atomic basis functions $\chi_A(\boldsymbol{r})$ centered at nucleus A (and their expansion coefficients C_A^i). Then, single components of $\rho(\boldsymbol{r})$ and $D(\boldsymbol{r})$ are expressed as

$$\rho^{(i)}(\boldsymbol{r}) \equiv n_i \sum_A^{\mathrm{AO}} |C_A^i|^2 \chi_A^2(\boldsymbol{r}) + n_i \sum_{A\neq B}^{\mathrm{AO}} C_A^{i*} C_B^i \chi_A(\boldsymbol{r})\chi_B(\boldsymbol{r}) \tag{27}$$

and

$$D^{(i)}(\boldsymbol{r}) \equiv n_i(2-n_i) \sum_A^{\mathrm{AO}} |C_A^i|^2 \chi_A^2(\boldsymbol{r}) + n_i(2-n_i) \times \sum_{A\neq B}^{\mathrm{AO}} C_A^{i*} C_B^i \chi_A(\boldsymbol{r})\chi_B(\boldsymbol{r}). \tag{28}$$

Since both n_i and $n_i(2-n_i)$ are positive semidefinite, their interatomic components

$$2n_i \mathrm{Re}\left(C_A^{i*} C_B^i\right)\chi_A(\boldsymbol{r})\chi_B(\boldsymbol{r}) \tag{29}$$

and

$$2n_i(2-n_i)\mathrm{Re}\left(C_A^{i*} C_B^i\right)\chi_A(\boldsymbol{r})\chi_B(\boldsymbol{r}) \tag{30}$$

should have the same sign; if one is positive (negative), the other must also be positive (negative). Nevertheless, in the total quantities summed over all the natural orbitals, the interatomic quantities

$$\rho_{AB}(\boldsymbol{r}) \equiv 2\left(\sum_i n_i \mathrm{Re}\left(C_A^{i*} C_B^i\right)\right)\chi_A(\boldsymbol{r})\chi_B(\boldsymbol{r}) \tag{31}$$

and

© Author(s) 2019

京都大学 KYOTO UNIVERSITY
A Self-archived copy in
Kyoto University Research Information Repository
https://repository.kulib.kyoto-u.ac.jp
京都大学学術情報リポジトリ KURENAI 紅 Kyoto University Research Information Repository

$$D_{AB}(\boldsymbol{r}) = 2\sum_i \left[n_i(2-n_i)\mathrm{Re}\left(C_A^{i*}C_B^i\right)\right]\chi_A(\boldsymbol{r})\chi_B(\boldsymbol{r}) \tag{32}$$

can have different signs. This is actually what we have observed in Fig. 8. In particular, for the highly energetic states [see panel (c) in Fig. 8], there are many bonding sites in which $\rho_{AB}(\boldsymbol{r}) > 0$ while $D_{AB}(\boldsymbol{r}) < 0$ with a large magnitude.

To illustrate how this situation can happen, let us suppose a diatomic molecule, say, A–B, having only two natural orbitals, one doubly occupied one $\lambda_1(\boldsymbol{r})$ ($n_1 = 2$) and the other a singly occupied $\lambda_2(\boldsymbol{r})$ ($n_2 = 1$). Besides that, assume that $\lambda_1(\boldsymbol{r})$ is bonding in A–B and $\lambda_2(\boldsymbol{r})$ is anti-bonding. Then, we have

$$\rho_{AB}(\boldsymbol{r}) \equiv 2\left[2\mathrm{Re}\left(C_A^{1*}C_B^1\right) + 1\mathrm{Re}\left(C_A^{2*}C_B^2\right)\right]\chi_A(\boldsymbol{r})\chi_B(\boldsymbol{r}), \tag{33}$$

while the unpaired electron density is merely

$$D_{AB}(\boldsymbol{r}) = 2\mathrm{Re}\left(C_A^{2*}C_B^2\right)\chi_A(\boldsymbol{r})\chi_B(\boldsymbol{r}). \tag{34}$$

Therefore, even if $\rho_{AB}(\boldsymbol{r})$ is positive, it can be expected that $D_{AB}(\boldsymbol{r})$ is negative. In this exemplified case, chemical bonding is conceived to be dominated by $\rho_{AB}(\boldsymbol{r}) > 0$, which gives rise to the accumulation of electron in between A and B. On the other hand, $D_{AB}(\boldsymbol{r}) < 0$ is a result of the anti-bonding nature of the singly occupied natural orbital $\lambda_2(\boldsymbol{r})$, which is supposed to push electrons back from the inter-atomic site to the atomic sites.

Another very significant characteristic of such anti-bonding orbitals is that they have far higher kinetic energy in the inter-atomic region. This is simply because the absolute value of the momentum of electrons, which is represented by

$$\left|\frac{\hbar}{i}\frac{\partial}{\partial x}\lambda_2(\boldsymbol{r})\right|, \tag{35}$$

is far larger in the interatomic site (recall the σ_u orbital of H_2) than the bonding orbitals (as in the σ_g orbital of H_2), for which one anticipates

$$\left|\frac{\hbar}{i}\frac{\partial}{\partial x}\lambda_2(\boldsymbol{r})\right| \sim 0, \tag{36}$$

where x indicates the inter-atomic distance. Therefore, the presence of the significantly negative unpaired electron density in the inter-atomic sites suggests that the relevant "bond energy" is higher (the potential basin is shallower) than that expected in terms of the positive value of $\rho_{AB}(\boldsymbol{r})$ alone.

To summarize, consider two chemical bonds, both of which have the same magnitude of $\rho_{AB}(\boldsymbol{r})$ but only one of which has negative $D_{AB}(\boldsymbol{r})$ of a large magnitude. Then, one may say that the strength of these chemical bonds, measured with the force constants that are by and large proportional to $\rho_{AB}(\boldsymbol{r})$, must be similar to each other but that the bond of a large negative $D_{AB}(\boldsymbol{r})$ should be significantly shallower and therefore must be less stable.

Returning to the B_{12} cluster of very high energies [like that presented in Fig. 8(c)], we may have a picture that shows many unpaired (radical) electrons are widely distributed in the many inter-atomic sites [see Fig. 10(a), right panel] bearing large kinetic energies. Such a view is consistent with what we observed in the shift of the virial value 2.0 to the smaller value [Fig. 7(c)], which suggests that the increase in the kinetic energy of electrons is due to the nonadiabatic interactions.

Also, the chemical bonds of shallower basin should lead to more frequent bond rearrangement (reconnection of the strings and webs) as is demonstrated in Fig. 9. This aspect will be discussed in future papers, in which we study the dynamical mechanism of the reconnection among the strings and webs.

V. HYPER-RESONANCE

This section is devoted to a rather conceptual discussion and analysis on the dynamical chemical bonding.

A. Notion of hyper-resonance proposed

"Resonance" is a technical term that is widely used in different contexts in very broad areas of science. Among others, particularly relevant to the present work, are the Pauling resonance in chemical electronic structure[8] and the Feshbach resonance[76] in quantum scattering theory.[77] The Pauling resonance can be viewed as a sort of configuration mixing (interaction) in terms of the so-called diabatic states (usually termed resonance structures) in the valence bond theory. The Feshbach resonance is temporary core-excited states promoted in a target particle (denoted as M) by the kinetic energy of an incident particle, say, A, the process of which is typically illustrated as

$$M + A \rightarrow (MA)^* \rightarrow \text{dissociations to energetically accessible channels.} \tag{37}$$

The diabatic representation often gives simpler interpretations both for the Pauling and Feshbach resonances, and yet they can be basically regarded as events on a single adiabatic potential surface.

By contrast, the electronic-nuclear non-Born–Oppenheimer states in the B_{12} cluster undergo very frequent transitions among adiabatic states. Mathematical manipulation to single out an adiabatic state is physically meaningful only for time-intervals as short as the femtosecond scale. A state prepared on a pure adiabatic state, which is possible only conceptually, diffuses very quickly in the electronic Hilbert space penetrating into other states as demonstrated in Fig. 4 (see also Fig. 12 in Ref. 44). The electronic state cannot remain in an isolated adiabatic surface and is forced to wander from one state to another visiting many states many times through the nonadiabatic interactions symbolically represented as

$$\sum_I^{\text{adiabatic}} C_I(t)\Phi_I^{\text{ad}}(\boldsymbol{r};\boldsymbol{R}(t)). \tag{38}$$

The electronic-state wandering motion among the adiabatic states is made possible by exchanging the energy with the complicated nuclear motions through their kinematic interactions, which may be regarded as resonance among the adiabatic states. These dynamical states can last for an extremely long time, during which the frequent reconnecting dynamics among chemical bonds takes place as illustrated in Fig. 9. Since each adiabatic state is already a Feshbach and/or Pauling resonance state, the present dynamics in B_{12} may be termed hyper-resonance (resonance among the resonant states).

B. Nonadiabatic transitions closing dissociation channels

To illustrate the effect of nonadiabatic interactions on the bonding structure of the B_{12} cluster and especially on the clear effect concerning the closing of dissociation channels, we compare

© Author(s) 2019

京都大学 KYOTO UNIVERSITY
A Self-archived copy in
Kyoto University Research Information Repository
https://repository.kulib.kyoto-u.ac.jp
京都大学学術情報リポジトリ KURENAI 紅 Kyoto University Research Information Repository

nonadiabatic dynamics with its adiabatic counterpart that is dissociating. For the present study, we do not aim to obtain a statistical sample but only a few representative trajectories for illustration. Pure adiabatic states are taken as initial states to highlight the mixing of states expected along the nonadiabatic trajectories. The time step taken is 0.01 fs for all trajectories. Unlike the set of trajectories given in Sec. IV, at each time step, the nuclear kinetic energy is scaled as to keep the total energy conserved (see the supplementary material for a discussion of the errors in the energy adjusted trajectories).

We obtain the initial conditions for a dissociating adiabatic trajectory by performing a "collision" and then reversing the process, as follows. An arbitrary nuclear geometry (which itself is taken from a previous nonadiabatic time evolution), with one of the nuclei placed 5 Å away from the rest of the cluster to represent a "dissociated" geometry [which is the same nuclear geometry shown in Fig. 11(a) for 100 fs], is taken as the initial geometry of an adiabatic time evolution, with 0.2 eV initial kinetic energy worth of momentum (sign taken arbitrarily) in each of the 11 × 3 degrees of freedom of the "bound" part of the cluster and a velocity of 0.1 Å fs^{-1} toward the center of mass for the three degrees of freedom of the "dissociated" nucleus. The translational momentum and total angular momentum of the cluster were adjusted to zero prior to time evolution. After an adiabatic time evolution of 100 fs, all signs of the momentum are reversed, and together with the nuclear geometry at that point, the obtained nuclear geometry and momentum serve as initial conditions for an adiabatic trajectory that will end in the dissociated geometry and one nucleus leaving the rest with a velocity of 0.1 Å fs^{-1} after 100 fs.

We computed adiabatic trajectories for the ground adiabatic electronic state (initial kinetic energy T_N = 9.48 eV and initial potential energy V = 17.58 eV for the dissociation trajectory) and for the adiabatic states 47 (initial T_N = 6.25 eV, V = 29.74 eV) and 303 (initial T_N = 9.82 eV, V = 50.07 eV). We note that for the ground state and state 47 trajectories, the adiabatic dissociation trajectory is the reverse of the adiabatic collision trajectory, as should be. For the state 303 trajectory, however, the electronic state self consistent field did not converge on a corresponding set of molecular orbitals after 40 fs on the "dissociation" trajectory.

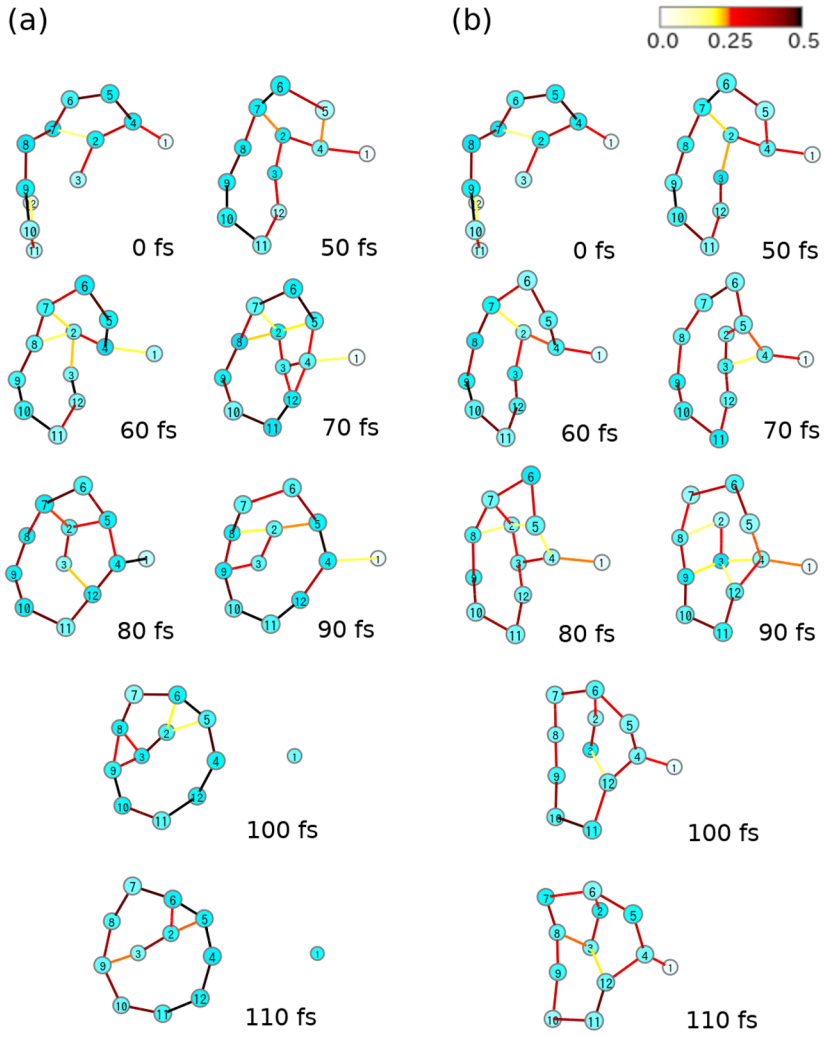

FIG. 11. B_{12} bonding structures along a trajectory under (a) adiabatic dynamics and (b) nonadiabatic dynamics, starting from the same initial conditions (initial adiabatic state 47). Time t in fs is indicated beside each structure. Structures are drawn and colored in the same way as in Fig. 9(a). At t = 110 fs, atom 1 is in the dissociation channel in the adiabatic dynamics, while this atom is pulled back to the cluster site in the nonadiabatic dynamics, thus evidencing that the dissociation channel is closed.

© Author(s) 2019

京都大学 KYOTO UNIVERSITY
A Self-archived copy in
Kyoto University Research Information Repository
https://repository.kulib.kyoto-u.ac.jp
京都大学学術情報リポジトリ KURENAI 紅 Kyoto University Research Information Repository

Nonadiabatic time evolutions were performed from the same initial conditions as the adiabatic dissociation trajectories to obtain nonadiabatic trajectories for comparison. For all three cases (ground electronic state and states 47 and 303), the resulting trajectories showed that the cluster remained bound 100 fs after the start of time evolution, evidencing that nonadiabatic interactions cause suppression of dissociation.

As an example in Fig. 11 a dissociating adiabatic trajectory on the adiabatic state 47 [Fig. 11(a)] is compared with a nonadiabatic trajectory from the same initial conditions [Fig. 11(b)]. The adiabatic trajectory results in dissociation. The nonadiabatic trajectory [Fig. 11(b)] is similar to the adiabatic trajectory up to 50 fs for this case, but after that the two trajectories deviate from each other. The nucleus that dissociates in the adiabatic trajectory remains bonded in the nonadiabatic trajectory.

Nonadiabatic trajectories starting from the nuclear geometry, momentum, and electronic state at 50 fs along the adiabatic dissociation trajectories were also computed (initial conditions closer to dissociation). For these initial conditions closer to dissociation, nonadiabatic trajectories starting from the adiabatic states 1 and 303 evolved in much the same ways (but not exactly the same) as the adiabatic trajectories and resulted in dissociation after all, but the state 47 nonadiabatic trajectory remained bound.

It is expected that the smaller clusters should have less dense quasi-degenerate electronic-state manifolds and weaker effect of the nonadiabatic transitions on closing dissociation channels. Therefore, adiabatic and nonadiabatic time evolutions of the B_6 cluster under similar conditions were also computed for various initial electronic states. It has turned out that they show the similar behavior to the B_{12} cases, that is, nonadiabatic trajectories do not dissociate easily despite dissociation of their adiabatic counterparts. Hence, we may conclude that the closing mechanism of dissociation channels by nonadiabatic transitions and thereby giving rise to long-lifetime is robust even for small boron clusters of the size down to B_6.

C. Phase-space volume for hyper-resonant states

As demonstrated above, the dissociation channels tend to be often closed by very frequent nonadiabatic transitions, resulting in very long lifetimes of these clusters. Our computational experience supports that this is indeed the case. Nevertheless, it is practically impossible to calculate the average lifetimes of the clusters as a function of energy given, for tracking the entire fate of the individual paths is inconceivably costly. Instead, we here make a simple statistical inference about possible elongation of the lifetimes in terms of a very primitive version of the phase-space theory of chemical reactions.

1. Lifetime on a single adiabatic potential energy surface

We here resort to a dramatically simplified statistical theory based on the phase space theory, originally proposed by Light.[78] The phase space theory has also been extensively applied in the context of cluster dynamics by the groups of Amar[79–81] and Calvo.[82–86] Fujii and Takatsuka have shown[87,88] how their refined phase space theory can accurately reproduce the rate in the (thermal) dissociation dynamics of $Ar_8 \to Ar_7 + Ar$ and $Ar_8 \to Ar_6 + Ar_2$. This study treats the dynamics on a single potential surface made up with the pairwise Morse potentials. By contrast, the present system B_{12} is much larger, and generation of each potential surface is, even if possible, too time-consuming to perform the statistical estimate of the relevant lifetime of a single cluster, let alone the computation of the phase-space volume for many nonadiabatically coupled densely quasi-degenerate electronic states. Therefore, the discussion made below is highly conceptual, and the dissociation probabilities of $B_{12} \to B_{11} + B$ are an estimate giving only the lowest bound.

The phase space theory of no external conditions imposed predicts the reaction rate k as

$$k = \frac{W_{N-1}(E)}{\Omega_N(E)}, \tag{39}$$

where $\Omega_N(E)$ and $W_{N-1}(E)$ are the density of the states of the N-particle cluster at the total energy E and the total flux induced by the dissociation of a single atom, respectively. For a single potential energy surface, say, $V_I(\boldsymbol{R})$, it is formally estimated with the expression

$$\Omega_N^{(I)}(E) = \hbar^{-3N} \int d\boldsymbol{R} d\boldsymbol{P}\, \delta(E - H_I(\boldsymbol{R}, \boldsymbol{P})), \tag{40}$$

where

$$H_I(\boldsymbol{R}, \boldsymbol{P}) = \frac{\boldsymbol{P} \cdot \boldsymbol{P}}{2} + V_I(\boldsymbol{R}), \tag{41}$$

with the obvious notation of the total nuclear momentum $\boldsymbol{P}$. Since there are not potential barriers like the transition state on $V_I(\boldsymbol{R})$ in the dissociation directions, the so-called dividing surface of $\Omega_N^{(I)}$, $\partial\Omega_N^{(I)}$, is not appropriately defined. In place of $\partial\Omega_N^{(I)}$, we use $\Omega_{N-1}^{(I)}(E - \Delta E)$, which is the phase space volume of the daughter cluster of $N - 1$ particles, with ΔE being the energy for a single dissociation particle to carry out of the parent cluster with the relative velocity $\vec{v}$. Then, the flux is here approximately expressed as

$$W_{N-1}^{(I)}(E) = \int \Omega_{N-1}^{(I)}(E - \Delta E)\vec{v}(\Delta E) \cdot d\vec{v}. \tag{42}$$

The reduced mass is set to be unity for simplicity. Thus, the critical quantity needed to estimate the statistical rate of the dissociation probability turns out to be the ratio

$$\frac{\Omega_{N-1}^{(I)}(E - \Delta E)}{\Omega_N^{(I)}(E)}. \tag{43}$$

We here assume that the phase space for B_{12} cluster under study has the mixing property and thereby is completely statistical (with no dynamical constraint like the presence of the tori). Then, we may regard the quantity

$$\Omega_N^{(I)}(E) - \Omega_{N-1}^{(I)}(E - \Delta E) \tag{44}$$

as the phase space volume for the trajectories that "tentatively" stay bound as B_{12}. The related entropy $s^{(I)}(E, \Delta E)$ can be defined as

$$s^{(I)}(E, \Delta E) = -\log\left(\frac{\Omega_N^{(I)}(E) - \Omega_{N-1}^{(I)}(E - \Delta E)}{\Delta\Omega}\right), \tag{45}$$

© Author(s) 2019

京都大学 KYOTO UNIVERSITY
A Self-archived copy in
Kyoto University Research Information Repository
https://repository.kulib.kyoto-u.ac.jp
京都大学学術情報リポジトリ KURENAI 紅 Kyoto University Research Information Repository

where $\Delta\Omega$ is meant to be the size of a unit cell of the phase space volume, such as $\hbar^{3N}$, in counting the number of cells included in the volume $\left[\Omega_N^{(I)}(E) - \Omega_{N-1}^{(I)}(E-\Delta E)\right]$.

2. Interconnection of the entire phase-space volume by the continual nonadiabatic contacts among the adiabatic phase spaces

The essential feature of our problem is that the potential surfaces, otherwise regarded as independent and isolated from each other, couple in a many to many manner through

$$-i\hbar\sum_{k=1}^{3N}\dot{R}_k(t)X_{IJ}^k(\boldsymbol{R}(t)) \tag{46}$$

and/or $H_{IJ}^{(\mathrm{el})}(\boldsymbol{R}(t))$ as in Eq. (5). Thus, at each phase space point $(\boldsymbol{R},\boldsymbol{P}) = \left(\boldsymbol{R},\dot{\boldsymbol{R}}\right)$, one state may remain as it is or make a transition to other states according to quantum mechanical probabilities. Thus, the state at $(\boldsymbol{R},\boldsymbol{P})$ may have multiple chances to choose the electronic states to branch to. If the transition among the electronic states was completely free with no restriction of the transition probabilities, the entropy confined in the individual state $s^{(I)}(E,\Delta E)$ should be relaxed to the sum of them such that

$$\begin{aligned} s^{(\max)}(E,\Delta E) &= \sum_I s^{(I)}(E,\Delta E) \\ &= -\sum_I \log\left(\frac{\Omega_N^{(I)}(E) - \Omega_{N-1}^{(I)}(E-\Delta E)}{\Delta\Omega}\right). \end{aligned} \tag{47}$$

In such an extreme case, therefore, the phase space volume is extended amounting to

$$\prod_I\left[\Omega_N^{(I)}(E) - \Omega_{N-1}^{(I)}(E-\Delta E)\right]. \tag{48}$$

On the other hand, the phase space volume directly connected to the dissociation channel should simply be the sum of each, that is,

$$\sum_I \Omega_{N-1}^{(I)}(E-\Delta E). \tag{49}$$

Hence, the dissociation probability can be dramatically lowered from the order of Eq. (43) to

$$\frac{\sum_I \Omega_{N-1}^{(I)}(E-\Delta E)}{\prod_I\left[\Omega_N^{(I)}(E) - \Omega_{N-1}^{(I)}(E-\Delta E)\right]} \tag{50}$$

in the extremum limit. Concomitantly, the lifetime of the cluster as estimated is expected to be by far longer than those of the hypothetical systems neglecting nonadiabatic interaction.

The above argument can be made a little more precise from the viewpoint of the number of periodic or quasi-periodic orbits involved in the phase space. Agung Budiyono *et al.* developed a semiclassical theory on enhancement of non-escape probability in open systems due to quantum localization induced by periodic orbits,[89] in which the physical situation studied is essentially the same as in the present case. Although their studied systems are very small, the conclusion drawn is general enough, that is, as the number of periodic (or quasi-periodic) orbits involved in phase space is larger, the dissociation probability is more suppressed in the exponential decay (dissociation) rate out of the system to an open channel. In a theoretical analogy, one can suppose that there are periodic orbits as many as N_I in the phase space of the size $\left[\Omega_N^{(I)}(E) - \Omega_{N-1}^{(I)}(E-\Delta E)\right]$ for $I = 1, 2, 3, \ldots$ in a simple manner that the number of periodic orbits is proportional to the phase space volume, that is,

$$\left[\Omega_N^{(I)}(E) - \Omega_{N-1}^{(I)}(E-\Delta E)\right] \propto N_I. \tag{51}$$

Take one of periodic orbits in the space I and J each. Assume that they have a nonadiabatic coupling somewhere at a point in $(\boldsymbol{R},\boldsymbol{P})$. For each orbit in I, there are two choices of path-branching; one remains on its own periodic trajectory, and the other penetrating into the periodic orbit on the Jth phase space. The same branching can take place in principle among the many coupled states, which result in the proliferation of the periodic orbits amounting at most to $N_1 \times N_2 \times N_3 \times \cdots$. Thus, we may expect

$$\prod_I N_I \to \prod_I\left[\Omega_N^{(I)}(E) - \Omega_{N-1}^{(I)}(E-\Delta E)\right]. \tag{52}$$

Once again, this estimate can be inserted in Eq. (50) to give a far smaller dissociation probability than the simple direct sum of the phase space volumes,

$$\sum_I\left[\Omega_N^{(I)}(E) - \Omega_{N-1}^{(I)}(E-\Delta E)\right]. \tag{53}$$

The present argument has been quite qualitative. A better estimate for more realistic phase-space volume could be made by taking an explicit account of the magnitude and phase-space distribution of the nonadiabatic coupling elements of Eq. (46).

VI. CONCLUSIONS

Nonadiabatic electron wavepacket dynamics in the densely quasi-degenerate electronic-state manifold of a boron cluster has been investigated as a prominent example of molecular properties that are rarely or never seen in the realm of the Born–Oppenheimer theoretical framework. Among others, the electronic states undergo extremely frequent nonadiabatic transitions, and thereby the notion of electronic state and chemical dynamics on isolated potential surfaces both lose sense. We thus have observed the very characteristic features of the novel chemical bonding of excited state boron clusters, some of which are summarized below.

1. Very frequent nonadiabatic transitions through numerous conical intersections and avoided crossings have been demonstrated in Fig. 4.
2. The dynamics of electronic energy associated with the fluctuation of chemical bonding, which is represented in terms of the electronic populations in the inter-atomic region, has been visualized (Fig. 6).
3. Electronic energy in the highly excited states deviates from the virial ratio 2 due to the presence of the nonadiabatic interactions (Fig. 7). The ratio is shifted to the increase in the kinetic energy and/or decrease in the electronic-nuclear potential energy. This is a physical manifestation of kinematic interaction between nuclei and electrons.

© Author(s) 2019

京都大学 KYOTO UNIVERSITY
A Self-archived copy in
Kyoto University Research Information Repository
https://repository.kulib.kyoto-u.ac.jp
京都大学学術情報リポジトリ KURENAI 紅 Kyoto University Research Information Repository

4. Characterization of the chemical bonding in the present cluster can be represented in terms of the notion of "string and web" (Fig. 9). These bonding structures keep reconnecting autonomously.
5. It has been found that the deeply negative values of the unpaired electron density lying in the inter-atomic bonding areas are also inherent to the chemical bonds in the highly excited states (Figs. 8 and 10). An interpretation of the role of the negative unpaired electron density has been discussed from the aspect of bond energy.
6. In order to quantify why and how the present cluster can have a very long lifetime even in their highly excited states, we have seen a numerical example of the role of nonadiabatic interaction that can close the dissociation channels (Fig. 11). A simple interpretation of the long lifetime is discussed in terms of the interconnection of phase-space volume that is brought about by the frequent and spatially widespread nonadiabatic couplings.
7. To comprehend these very characteristic properties, we have proposed the notion of hyper-resonance.

In our future paper, we plan to analyze the dynamical mechanism of reconnection of the "string and web," which should provide a key for the study of the reactivity inherent to highly quasi-degenerate nonadiabatic electronic states. A study is also under way in our laboratory, in which guest molecules are included into boron clusters which are supposed to provide a very characteristic reaction field.

SUPPLEMENTARY MATERIAL

See supplementary material for the justification of only including excitation from the HOMO as the configuration interaction active space and for a discussion on the energy adjusted trajectories in Sec. V B.

ACKNOWLEDGMENTS

The work has been supported by JSPS KAKENHI, the Grant No. JP15H05752.

REFERENCES

[1]T. Helgaker, P. Jørgensen, and J. Olsen, *Molecular Electronic-Structure Theory* (John Wiley, New York, 2002).
[2]I. Mayer, *Simple Theorems, Proofs, and Derivations in Quantum Chemistry* (Kluwer Academic, New York, 2003).
[3]*Conical Intersections: Electronic Structure, Dynamics and Spectroscopy*, edited by W. Domcke, D. Yarkony, and H. Köppel (World Scientific, New Jersey, 2004).
[4]M. Baer, *Beyond Born–Oppenheimer: Electronic Nonadiabatic Coupling Terms and Conical Intersections* (Wiley, New Jersey, 2006).
[5]H. Nakamura, *Nonadiabatic Transition: Concepts, Basic Theories and Applications*, 2nd ed. (World Scientific, Singapore, 2012).
[6]T. Yonehara, K. Hanasaki, and K. Takatsuka, Chem. Rev. **112**, 499 (2012).
[7]K. Takatsuka, T. Yonehara, K. Hanasaki, and Y. Arasaki, *Chemical Theory Beyond the Born–Oppenheimer Paradigm* (World Scientific, Singapore, 2015).
[8]L. Pauling, *The Nature of the Chemical Bond and the Structure of Molecules and Crystals*, 3rd ed. (Cornell University Press, Ithaca, 1960).
[9]A. Zewail, *Femtochemistry: Ultrafast Dynamics of the Chemical Bond* (World Scientific, Singapore, 1994), Vols. 1 and 2.
[10]An extensive review is given by F. Krausz and M. Ivanov, Rev. Mod. Phys. **81**, 163 (2009).
[11]Y. Arasaki, Y. Mizuno, S. Scheit, and K. Takatsuka, J. Chem. Phys. **144**, 044107 (2016).
[12]W. N. Lipscomb, J. Chem. Phys. **22**, 985 (1954).
[13]W. H. Eberhardt, B. Crawford, and W. N. Lipscomb, J. Chem. Phys. **22**, 989 (1954).
[14]W. N. Lipscomb, *Boron Hydrides* (W. A. Benjamin, New York, 1963).
[15]W. N. Lipscomb, Science **153**, 373 (1966).
[16]W. N. Lipscomb, Science **196**, 1047 (1977).
[17]R. B. King, Chem. Rev. **101**, 1119 (2001).
[18]H. C. Brown, Tetrahedron **12**, 117 (1961).
[19]H. C. Brown, *Organic Syntheses via Boranes* (Wiley-Interscience, New York, 1975).
[20]J. W. B. Fyfe and A. J. B. Watson, Chem **3**, 31 (2017).
[21]D. Olid, R. Núñez, C. Viñas, and F. Teixidor, Chem. Soc. Rev. **42**, 3318 (2013).
[22]Q. Weng, X. Wang, X. Wang, Y. Bando, and D. Golberg, Chem. Soc. Rev. **45**, 3989 (2016).
[23]B. P. Dash, R. Satapathy, J. A. Maguire, and N. S. Hosmane, New J. Chem. **35**, 1955 (2011).
[24]Y. Su and R. Kinjo, Coord. Chem. Rev. **352**, 346 (2017).
[25]Y. Fang and X. Wang, Angew. Chem., Int. Ed. **56**, 15506 (2017).
[26]J. Nagamatsu, N. Nakagawa, T. Muranaka, Y. Zenitani, and J. Akimitsu, Nature **410**, 63 (2001).
[27]S. Souma, Y. Machida, T. Sato, T. Takahashi, H. Matsui, S.-C. Wang, H. Ding, A. Kaminski, J. C. Campuzano, S. Sasaki, and K. Kadowaki, Nature **423**, 65 (2003).
[28]P. Qi, Y. Zhang, and H. Chen, Comput. Theor. Chem. **1047**, 30 (2014).
[29]S. Mukherjee and P. Thilagar, Chem. Commun. **52**, 1070 (2016).
[30]C. Viñas, F. Teixidor, and R. Núñez, Inorg. Chim. Acta **409**, 12 (2014).
[31]T. J. Carter, R. Mohtadi, T. S. Arthur, F. Mizuno, R. Zhang, S. Shirai, and J. W. Kampf, Angew. Chem., Int. Ed. **53**, 3173 (2014).
[32]D. B. Diaz and A. K. Yudin, Nat. Chem. **9**, 731 (2017).
[33]H. S. Ban and H. Nakamura, Chem. Rec. **15**, 616 (2015).
[34]L.-S. Wang, Int. Rev. Phys. Chem. **35**, 69 (2016).
[35]S. Jalife, L. Liu, S. Pan, J. L. Cabellos, E. Osorio, C. Lu, T. Heine, K. J. Donald, and G. Merino, Nanoscale **8**, 17639 (2016).
[36]A. C. Reber and S. N. Khanna, J. Chem. Phys. **142**, 054304 (2015).
[37]A. P. Sergeeva, I. A. Popov, Z. A. Piazza, W.-L. Li, C. Romanescu, L.-S. Wang, and A. I. Boldyrev, Acc. Chem. Res. **47**, 1349 (2014).
[38]E. Oger, N. R. M. Crawford, R. Kelting, P. Weis, M. M. Kappes, and R. Ahlrichs, Angew. Chem., Int. Ed. **46**, 8503 (2007).
[39]D. Y. Zubarev and A. I. Boldyrev, J. Comput. Chem. **28**, 251 (2007).
[40]A. N. Alexandrova, A. I. Boldyrev, H.-J. Zhai, and L.-S. Wang, Coord. Chem. Rev. **250**, 2811 (2006).
[41]S. R. Reddy and S. Mahapatra, J. Chem. Phys. **136**, 024323 (2012).
[42]T. Yonehara and K. Takatsuka, J. Chem. Phys. **137**, 22A520 (2012).
[43]Z. Li, T. Yonehara, and K. Takatsuka, Chem. Phys. **464**, 14 (2016).
[44]T. Yonehara and K. Takatsuka, J. Chem. Phys. **144**, 164304 (2016).
[45]K. Takatsuka, J. Phys. Chem. A **111**, 10196 (2007).
[46]T. Yonehara and K. Takatsuka, J. Chem. Phys. **129**, 134109 (2008).
[47]K. Hanasaki and K. Takatsuka, Phys. Rev. A **81**, 052514 (2010).
[48]K. Takatsuka and T. Yonehara, Phys. Chem. Chem. Phys. **13**, 4987 (2011).
[49]T. Yonehara and K. Takatsuka, J. Chem. Phys. **128**, 154104 (2008).
[50]K. Takatsuka and T. Yonehara, Adv. Chem. Phys. **144**, 93 (2010).
[51]T. Yonehara and K. Takatsuka, J. Chem. Phys. **132**, 244102 (2010).
[52]K. Takatsuka, J. Chem. Phys. **147**, 174102 (2017).
[53]K. Takatsuka, J. Phys. B: At., Mol. Opt. Phys. **47**, 124038 (2014).
[54]T. Matsuoka and K. Takatsuka, J. Chem. Phys. **146**, 134114 (2017).
[55]T. Matsuoka and K. Takatsuka, J. Chem. Phys. **148**, 014106 (2018).

© Author(s) 2019

京都大学 KYOTO UNIVERSITY
A Self-archived copy in
Kyoto University Research Information Repository
https://repository.kulib.kyoto-u.ac.jp
京都大学学術情報リポジトリ KURENAI 紅 Kyoto University Research Information Repository

[56]K. Takatsuka, J. Chem. Phys. **146**, 084312 (2017).
[57]T. Yonehara, S. Takahashi, and K. Takatsuka, J. Chem. Phys. **130**, 214113 (2009).
[58]K. Takatsuka, Chem. Phys. **515**, 52 (2018).
[59]Y. Arasaki, K. Takatsuka, K. Wang, and V. McKoy, Phys. Rev. Lett. **90**, 248303 (2003); J. Chem. Phys. **119**, 7913 (2003).
[60]A. J. Jenkins, K. E. Spinlove, M. Vacher, G. A. Worth, and M. A. Robb, J. Chem. Phys. **149**, 094108 (2018).
[61]M. Vacher, M. J. Bearpark, and M. A. Robb, Theor. Chem. Acc. **135**, 187 (2016).
[62]M. Vacher, D. Mendive-Tapia, M. J. Bearpark, and M. A. Robb, J. Chem. Phys. **142**, 094105 (2015).
[63]M. Vacher, D. Mendive-Tapia, M. J. Bearpark, and M. A. Robb, Theor. Chem. Acc. **133**, 1505 (2014).
[64]D. Mendive-Tapia, M. Vacher, M. J. Bearpark, and M. A. Robb, J. Chem. Phys. **139**, 044110 (2013).
[65]W. C. Swope, H. C. Andersen, P. H. Berens, and K. R. Wilson, J. Chem. Phys. **76**, 637 (1982).
[66]M. W. Schmidt, K. K. Baldridge, J. A. Boatz, S. T. Elbert, M. S. Gordon, J. H. Jensen, S. Koseki, N. Matsunaga, K. A. Nguyen, S. Su, T. L. Windus, M. Dupuis, and J. A. Montgomery, J. Comput. Chem. **14**, 1347 (1993).
[67]K. Takatsuka, T. Fueno, and K. Yamaguchi, Theor. Chim. Acta **48**, 175 (1978).
[68]K. Ruedenberg, Rev. Mod. Phys. **34**, 326 (1962).
[69]W. J. Hehre, R. F. Stewart, and J. A. Pople, J. Chem. Phys. **51**, 2657 (1969).
[70]R. Bowen, Am. J. Math. **92**, 725 (1970).
[71]J. Guckenheimer and P. Holmes, *Nonlinear Oscillations, Dynamical Systems, and Bifurcations of Vector Fields* (Springer, New York, 1983).
[72]J. Hubbard, Proc. R. Soc. London, Ser. A **276**, 238 (1963).
[73]G. B. Bacskay, S. Nordholm, and K. Ruedenberg, J. Phys. Chem. A **122**, 7880 (2018).
[74]R. Matsuzaki and K. Takatsuka, J. Comput. Chem. **40**, 148 (2019).
[75]R. Matsuzaki and K. Takatsuka, J. Chem. Phys. **150**, 014103 (2019).
[76]H. Feshbach, Ann. Phys. **19**, 287 (1962).
[77]R. G. Newton, *Scattering Theory of Waves and Particles* (Springer, Berlin, 1982).
[78]J. C. Light, J. Chem. Phys. **40**, 3221 (1964).
[79]S. Weerasinghe and F. G. Amar, J. Chem. Phys. **98**, 4967 (1993).
[80]P. Parneix, P. Bréchignac, and F. G. Amar, J. Chem. Phys. **104**, 983 (1996).
[81]P. Parneix, F. G. Amar, and P. Bréchignac, Chem. Phys. **239**, 121 (1998).
[82]F. Calvo and P. Labastie, Eur. Phys. J. D **3**, 229 (1998).
[83]F. Calvo, J. Phys. Chem. B **105**, 2183 (2001).
[84]F. Calvo and P. Parneix, J. Chem. Phys. **119**, 256 (2003).
[85]P. Parneix and F. Calvo, J. Chem. Phys. **119**, 9469 (2003).
[86]F. Calvo and P. Parneix, J. Chem. Phys. **120**, 2780 (2004).
[87]M. Fujii and K. Takatsuka, J. Phys. Chem. A **111**, 1389 (2007).
[88]M. Fujii and K. Takatsuka, J. Chem. Phys. **128**, 114318 (2008).
[89]A. Budiyono, T. Kato, K. Takatsuka, and K. Nakamura, Phys. Lett. A **367**, 331 (2007).

© Author(s) 2019